8-2011

The Role of Cancer-Associated Fibroblasts in Lung Tumorigenesis

Jonathon D. Roybal

Recommended Citation

The Role of Cancer-Associated Fibroblasts in Lung Tumorigenesis

By

Jonathon D. Roybal, M.S.

APPROVED:

_____
Dr. Jonathan M. Kurie, M.D.
Supervisory Professor

_____
Dr. Pierre McCrea, Ph.D.

_____
Dr. Faye M. Johnson, M.D., Ph.D.

_____
Dr. Yang Xia, M.D., Ph.D.

_____
Dr. Ja Seok Peter Koo, Ph.D.

APPROVED:

_____
Dr. George M. Stancel, Ph.D.
Dean, The University of Texas Health Center at Houston
Graduate School of Biomedical Sciences

Development of an *In Vitro* Model to Study Tumor Cell-Fibroblast Interactions in Lung
Cancer Metastasis

A

DISSERTATION

Presented by the Faculty of the

University of Texas Health Center at Houston

And

The University of Texas

M.D. Anderson Cancer Center

Graduate School of Biomedical Sciences

In Partial Fulfillment

of the Requirements

for the Degree of

DOCTOR OF PHILOSOPHY

By

Jonathon D. Roybal, B.S., M.S.

Houston, Texas

August 2011

Acknowledgements

There are many people here at the U.T. M.D. Anderson Cancer Center to thank for their contributions toward my success and for making me a better scientist. Their continual guidance, inspiration, and support have led me to where I am today and to where I am going in the future.

I would like to take this opportunity to thank Dr. Jonathan M. Kurie M.D., my supervisor and chair of my advisory and supervisory committee, for allowing me to do lung cancer research in his laboratory and for inspiring me to make a difference in cancer research. He has really helped me to come far in my academic career; not only has he led me down a path that makes science unequivocally interesting, but also he has encouraged me to think independently and to generate novel hypotheses. He has demonstrated the importance of taking what we discover at the bench out of the lab context and back to the bedside in the clinic. As a physician scientist at M.D. Anderson, he has been a great mentor not only in helping me to develop my thinking processes but also in modeling the dedication and hard work that it takes to fund the lab and create opportunities for us to pursue exciting and novel projects in the field of lung cancer research. His many hours of writing grants do not go unnoticed in the Kurie lab; we are extremely grateful for all of his efforts.

or concern with the experiments. Dr. Ahn's skills in molecular biology have been invaluable to this project by creating the site-directed mutagenesis clones and 3'-UTR assays that demonstrated VEGFR1 is a direct target of miR-200. Dr. Zhang aided in the testing of the VEGFR1 clones that helped to facilitate the quick movement toward publication of this work. Both these post-doctoral fellows were key in publishing this work and key to the development of myself as a scientist.

Dr. Don L. Gibbons M.D., Ph.D. has been a great asset and collaborator in my project. His work in the generation of the metastatic cell lines was foundational to my project, because without these valuable tools I would not have been able to study murine metastatic lung cancer. He has also been there on a daily basis to discuss experiments and ideas, which I found to be invaluable. When I was thinking about one step in my project, he persistently encouraged and challenged me to think beyond that one step to think of the next three that followed, which has taught me to broaden and consider the scope of my project. Not only has he been there to guide me scientifically, but he also has been there as a friend with advice, for which I am extremely grateful. It has been great to work with him, and I know he will be successful at his new appointment as faculty in the department of Thoracic Head and Neck Medical Oncology at M.D. Anderson.

and stipend, and to reach my goals without having to worry about the financial burden of school loans.

Last but not least I would like to thank my friends and family for their continued encouragement and support of my dreams and goals. When I thought that things were getting tough they were always there to help me and make me realize that problems are present in every occupation and that dealing with them in a positive manner is the best strategy. Their continued positive attitudes and energy have helped me to get to where I am today.

The Role of Cancer-Associated Fibroblasts in Lung Tumorigenesis.

Publication No._____

Jonathon D. Roybal, M.S.

Supervisory Professor: Dr. Jonathan M. Kurie, M.D.

Abstract

The extracellular milieu is rich in growth factors that drive tumor progression,
but the mechanisms that govern tumor cell sensitivity to those ligands have not
been fully defined. In this study, we address this question in mice that develop
metastatic lung adenocarcinomas through the suppression of the microRNA-
200 (miR-200) family. Cancer-associated fibroblasts (CAF) enhance tumor
growth and invasion by secreting VEGF-A that binds to VEGFR1, a process
required for tumor growth and metastasis in mice and correlated with a poor
prognosis in lung adenocarcinoma patients. In this study, we discovered that
miR-200 blocked CAF-induced tumor cell invasion by directly targeting
VEGFR1 in tumor cells. In the context of previous studies, our findings suggest
that the miR-200 family is a point of convergence for diverse biologic processes
that regulate tumor cell proliferation, invasion, and metastasis; its target genes

drive epithelial-to-mesenchymal transition (*ZEB1* and *ZEB2*) and promote

sensitivity to a potent tumor growth factor emanating from the microenvironment

(VEGFR1). Clinical trials should focus not only on the role of VEGFR1 in

angiogenesis but also on the expression and activation of VEGFR1 in tumor

cells by stromal sources of VEGF-A in the tumor microenvironment as a target

for metastasis prevention.

TABLE OF CONTENTS   **PAGE**

LIST OF ILLUSTRATIONS **PAGE**

LIST OF TABLES

LIST OF ABBREVIATIONS

APC	Allophycocyanin
bp	Base Pairs
BM	Bone Marrow
BSA	Bovine Serum Albumin
CAF	Cancer-Associated Fibroblast
CCL2/MCP-1	Chemokine (C-C motif) Ligand 2
CCL3/MIP-1α	Chemokine (C-C motif) Ligand 3
CCL4/MIP-1β	Chemokine (C-C motif) Ligand 4
CCR1	Chemokine (C-C motif) Receptor 1
CCR2	Chemokine (C-C motif) Receptor 2
CCR5	Chemokine (C-C motif) Receptor 5
cDNA	Complimentary Deoxyribonucleic Acid
Col1	Collagen Type 1
CXCL1/KC	Chemokine (C-X-C motif) Ligand 1
CXCL2/MIP2	Chemokine (C-X-C motif) Ligand 2
CXCL9/MIG	Chemokine (C-X-C motif) Ligand 9
CXCR2	Chemokine (C-X-C motif) Receptor 2
CXCR4	Chemokine (C-X-C motif) Receptor 4
DNA	Deoxyribonucleic Acid
dsRNA	Double-stranded Ribonucleic Acid
EMT	Epithelial-to-Mesenchymal Transition

ETBR	Ethidium Bromide
EDTA	Ethylenediaminetetraacetic Acid
EYFP	Enhanced Yellow Fluorescence Protein
FACS	Fluorescence-activated cell sorting
FSP1	Fibroblast Specific Protein 1
GFR	Growth Factor Reduced
HBSS	Hank's Buffered Salt Solution
IACUC	Institutional Animal Care and Use Committee
IgG	Immunoglobulin G
IL-6	Interleukin-6
IL-6Rα	Interleukin-6 Receptor Alpha
IL-18R1	Interleukin-18 Receptor 1
M-CSF	Marcophage Colony Stimulating Factor
LF	Lung Fibroblasts
mRNA	Messenger Ribonucleic Acid
miRNA	MicroRNA
miR-200	MicroRNA-200
NIH	National Institutes of Health
NSCLC	Non-small Cell Lung Cancer
PBS	Phosphate Buffered Saline
PBS-T	Phosphate Buffered Saline-Tween
PCR	Polymerase Chain Reaction
RBC	Red Blood Cells

qPCR	Quantitative Real-Time Polymerase Chain Reaction
RNA	Ribonucleic acid
shRNA	Short-Hairpin Ribonucleic Acid
TBI	Total-body Irradiation
TBST	Tris-Buffered Saline Tween-20
TGF-β1	Transforming Growth Factor Beta 1
TGF-βR1	Transforming Growth Factor Beta Receptor 1
TGF-βR2	Transforming Growth Factor Beta Receptor 2
UTR	Untranslated Region
UV	Ultraviolet
VEGF	Vascular Endothelial Growth Factor
VEGF-A	Vascular Endothelial Growth Factor A
VEGFR1/Flt1	Vascular Endothelial Growth Factor Receptor 1
VEGFR3/Flt4	Vascular Endothelial Growth Factor Receptor 3
VHL	Von Hippel-Lindau Tumor Suppressor
Zeb1	Zinc Finger E-box Binding Homeobox 1
Zeb2	Zinc Finger E-box Binding Homeobox 2

Chapter One

Introduction

Lung Cancer

According to the 2008 cancer statistics, cancer is the second leading cause of death in the U.S. following heart disease, with little improvement over the past thirty years for overall-survival with current modalities for treatment and prevention (Jemal et al., 2010a; Jemal et al., 2010b). Cancer arising in the lung and bronchus is the second highest in estimated new cases (116,750 male and 105,770 female) of the ten leading cancer types and the leading cause of estimated deaths for 2010 (86,200 male and 71,080 female, Figure 1A)(Jemal et al., 2010b). The estimated 2010 statistics clearly demonstrate that the annual age-adjusted cancer death rates from 1930 to 2006 have shown little significant improvement in the treatment of lung cancer in females, with only a marginal improvement in males (Jemal et al., 2010b). At time of diagnosis, patients with lung cancer typically present advanced late-stage metastatic disease that is inoperable and has the smallest chance of survival out of all the stages (localized, regional, and distant, Figure 1B and 1C)(Jemal et al., 2010b). Lung-cancer diagnosis and treatments have not improved over the past thirty years for two reasons: not only do we currently lack tools and animal models that represent the metastatic disease seen in advance-staged lung cancer patients, but also we need more detailed knowledge of the tumor microenvironment to understand the disease and the molecular switches regulated by the different components (i.e. different cells, soluble-secreted proteins, extracellular matrix, etc.).

A

Estimated New Cases*

	Males				Females		
Prostate	217,730	28%		Breast	207,090	28%
Lung & bronchus	116,750	15%		Lung & bronchus	105,770	14%
Colon & rectum	72,090	9%		Colon & rectum	70,480	10%
Urinary bladder	52,760	7%		Uterine corpus	43,470	6%
Melanoma of the skin	38,870	5%		Thyroid	33,930	5%
Non-Hodgkin lymphoma	35,380	4%		Non-Hodgkin lymphoma	30,160	4%
Kidney & renal pelvis	35,370	4%		Melanoma of the skin	29,260	4%
Oral cavity & pharynx	25,420	3%		Kidney & renal pelvis	22,870	3%
Leukemia	24,690	3%		Ovary	21,880	3%
Pancreas	21,370	3%		Pancreas	21,770	3%
All Sites	**789,620**	**100%**		**All Sites**	**739,940**	**100%**

Estimated Deaths

	Males				Females		
Lung & bronchus	86,220	29%		Lung & bronchus	71,080	26%
Prostate	32,050	11%		Breast	39,840	15%
Colon & rectum	26,580	9%		Colon & rectum	24,790	9%
Pancreas	18,770	6%		Pancreas	18,030	7%
Liver & intrahepatic bile duct	12,720	4%		Ovary	13,850	5%
Leukemia	12,660	4%		Non-Hodgkin lymphoma	9,500	4%
Esophagus	11,650	4%		Leukemia	9,180	3%
Non-Hodgkin lymphoma	10,710	4%		Uterine Corpus	7,950	3%
Urinary bladder	10,410	3%		Liver & intrahepatic bile duct	6,190	2%
Kidney & renal pelvis	8,210	3%		Brain & other nervous system	5,720	2%
All Sites	**299,200**	**100%**		**All Sites**	**270,290**	**100%**

FIGURE 1. Ten Leading Cancer Types for the Estimated New Cancer Cases and Deaths by Sex, 2010.
*Excludes basal and squamous cell skin cancers and in situ carcinoma except urinary bladder. Estimates are rounded to the nearest 10.

B

Lung and Bronchus

C

Lung and Bronchus
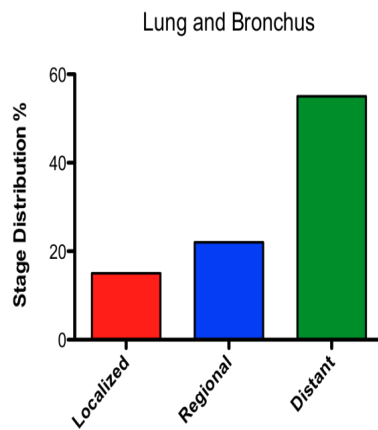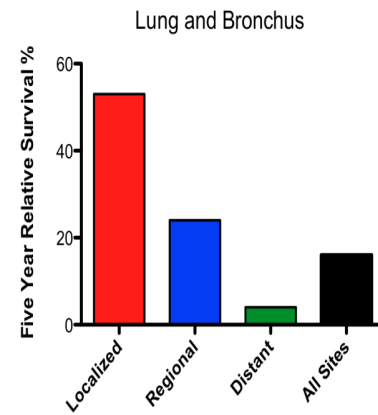
Figure 1: Lung Cancer Statistics.
(A) Depicts the ten leading cancer types for the estimated new cases and **(B)** deaths by gender for the year 2010. **(C)** The stage distribution of selected cancers by race at diagnosis within the United States from the year 1999 to 2005. **(D)** The five-year relative survival rates among patients diagnosed with selected cancers stage at diagnosis and race within the United States from the year 1999 to 2006.
Adapted from: Jemal 2010.

A Model of Advanced Lung Cancer Disease

Fortunately in more recent years researchers have created a lung cancer mouse model that develops advanced lung adenocarcinomas with defined metastatic potential, hereafter termed K-ras;p53 mutant mice (Gibbons et al., 2009a; Roybal et al., 2011). These mice express two specific mutations: a common Li-Fraumeni Tp53 mutation (p53^{R172H}) found in Li-Fraumeni patients and a K-ras (K-ras^{G12D}) mutation that results in sporadic lung cancers that develop metastatic disease. Expression profiling of the tumors from these mice has demonstrated an analog between the mice and a subset of NSCLC patients with a poor prognosis (Gibbons et al., 2009a). These genetically engineered mouse models are valuable tools that allow researchers to study the genetic effects that promote metastatic lung disease and test an array of hypotheses that could lead to potential therapeutics for the treatment of the disease. This model is very robust not only because of its genetic background but also because the mice are immunocompetent, allowing the mice to undergo normal immunological responses, which permit researchers to survey the local and metastatic tumor microenvironment *in vivo*.

The Tumor Microenvironment

Within the tumor microenvironment, a great deal of changes can occur in response to various cell types (i.e. fibroblasts, endothelial cells, macrophage, etc.), secreted soluble/diffusible factors (cytokines, chemokines, and growth factors), and structural extracellular matrix proteins (collagen, elastin,

fibronectin, etc.) that can influence the tumor and the surrounding stroma
(Figure 2). Previous studies have clearly demonstrated that the infiltrating
activated stromal cells can govern the metastatic potential of cancer cells by
secreting a number of soluble factors within the microenvironment; these
soluble factors then bind to cognate receptors on cancer cells causing
inflammation, cell proliferation, and a number of other tumor-promoting events
(Roybal et al., 2011). Despite knowing how secreted soluble factors influence
other types of cancers the cytokine milieu has not been fully elucidated in
metastatic NSCLC.

One of these activated stromal cells, a polarized M2 macrophage, has
been shown to promote tumor progression (Mantovani et al., 2004; Mantovani
et al., 2002). The activation of the M2 macrophage from the M1 macrophage,
which aids in the immune response and is non-tumor promoting, is due in part
to the cytokine milieu present within the tumor microenvironment. In addition to
these macrophages, fibroblasts within the local and tumor microenvironment
also secrete soluble factors and produce the extracellular matrix that governs
the niche.

Fibroblasts and Cancer

A growing body of evidence suggests that metastasis is regulated by
cells involved in inflammation, angiogenesis, and structural remodeling;
however, the role of fibroblasts in metastatic NSCLC cancer has not been fully
elucidated (Shimoda et al.; Wu and Zhou, 2009; Zhou et al., 2006).
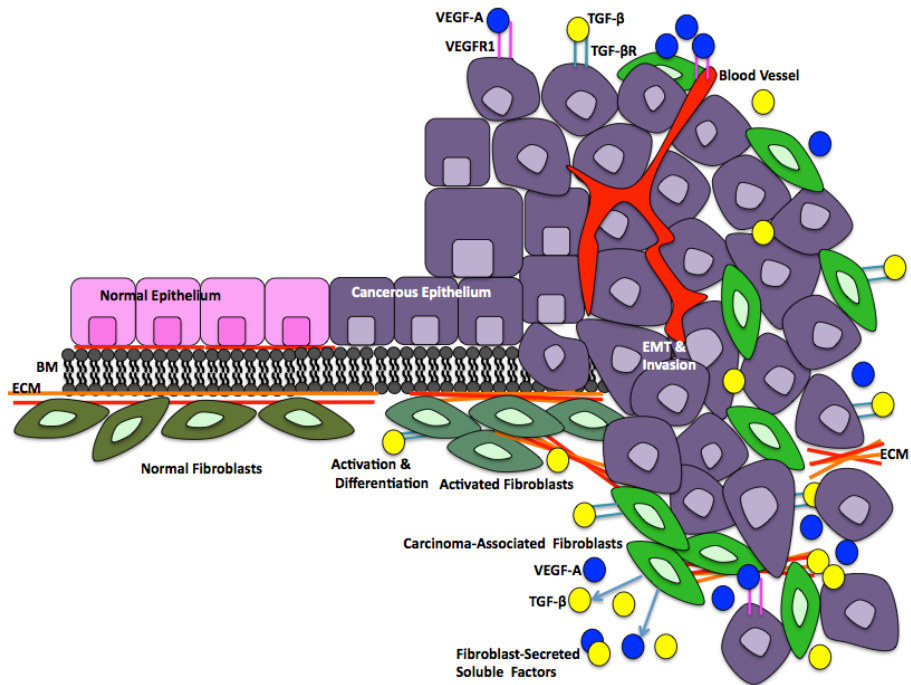
Figure 2: The Tumor Microenvironment.
Schematic representation of the biologic activities within the tumor
microenvironment. Fibroblasts (highlighted in red boxes), the cell of interest
in our research goals, are depicted as non-tumorigenic fibroblasts
(Fibroblasts) that transition to activated fibroblasts, which ultimately lead to
pro-tumorigenic carcinoma-associated fibroblasts (CAF). This figure also
shows VEGF-A and its receptor VEGFR-1 as contributing to the tumor
microenvironment. Soluble-secreted factors are capable of eliciting multiple
effects within the tumor microenvironment; the figure depicts TGF-β causing
cells to undergo EMT/invasion and proliferation/differentiation of CAF.

Central to these processes are cancer-associated fibroblasts (CAF), which were

initially described as myofibroblasts; however, not all CAF have these features

(Desmouliere et al., 2004; Sugimoto et al., 2006). CAF have multiple cells-of-

origin, including resident fibroblasts, endothelial cells, adipocytes, and bone

marrow-derived mesenchymal cells (Wu and Zhou, 2009). CAF play a

functional role in tumor progression as shown by genetic and pharmacologic

approaches to eradicate CAF in mice and by studies on human primary tumors

that have correlated CAF gene expression with a poor prognosis (Chang et al.,

2004; Santos et al., 2009). CAFs promote tumorigenesis by recruiting

macrophages and suppressing T cell anti-tumor immunity (Erez et al.; Nazareth

et al., 2007). These cells interact through paracrine mechanisms by secreting

matrix metalloproteinases and ligands for growth factor receptors, interleukin

receptors, CC chemokine receptors, CXC chemokine receptors, and other

factors (Wu and Zhou, 2009; Erez et al.; Anderberg et al., 2009). Although

many of these proteins bind directly to receptors on tumor cells and may

thereby control tumor progression, little is known about the mechanisms that

regulate tumor cell sensitivity to those cytokines.

miR-200 and Metastasis

Recent studies, ranging in multiple organ types and systems in cancer,

have provided evidence that miRNA are capable of governing cellular

processes that promote or aid tumorigenesis and metastases (Gibbons et al.,

2009b). miRNA are small, single-stranded, non-coding RNA gene products

(19-25 nucleotide bases in length) formed from double-stranded RNA (dsRNA) that are processed from an immature form to a mature miRNA in order to regulate gene expression (Shenouda and Alahari, 2009; Carletti and Christenson, 2009). The mature miRNA binds onto the 3' untranslated region (3'-UTR) on the target messenger RNA (mRNA), thereby regulating gene expression either by controlling translational efficiency or by degrading the transcript. More specifically, miR-200 is one family of miRNA that has been shown to be regulated by Zeb1 and Zeb2 transcription factors, which decrease miR-200 levels, promote metastases, and induce EMT (epithelial to mesenchymal transformation) under TGF-β stimulation (Gibbons et al., 2009b; Wipff et al., 2007). Additionally low expression levels of miR-200b, one of the five miR-200 family members, has been correlated to a specific subset of lung adenocarcinoma patients and predicts a high probability of recurrence of disease. Although we know that miR-200 is a central regulator of metastasis, the current evidence demonstrates a critical need to identify miR-200 target genes involved in this process and its role within the tumor microenvironment. This study postulates that miR-200 targets cell surface receptors that transmit paracrine signals from the microenvironment. A CAF population was isolated from lung adenocarcinomas in mice by using antibodies against Thy-1 (CD90), a cell surface glycoprotein that is expressed primarily on lung fibroblasts, neural cells, and leukocytes (Rege and Hagood, 2006; Hardie et al., 2009). Findings from these studies revealed sharp differences between CAF and their normal lung tissue counterpart; the CAF had more prominent interactions with tumor

cells driven in part by secretion of vascular endothelial growth factor-A (VEGF-A), which enhanced tumor cell proliferation and invasion. Tumor cells blocked their interactions with CAF through miR-200, which directly targeted VEGFR1(*Flt1*) in tumor cells. These findings demonstrate a novel role for miR-200 in the regulation of tumor cell sensitivity to a paracrine signal emanating from the microenvironment.

Significance

In the context of what has been reported previously, the findings presented here suggest that the microRNA-200 family (miR-200) is a point of convergence for diverse biologic processes. The upregulation of its target genes *ZEB1* and *ZEB2* drive epithelial-to-mesenchymal transition (EMT), and increased expression of VEGFR1 promotes sensitivity to VEGF-A, all of which regulate tumor cell proliferation, invasion, and metastasis. Although its role in angiogenesis has been the focus of clinical trials, VEGFR1 expression in tumor cells and its activation by cellular sources (i.e. epithelial cells or stromal cells such as CAFs) of VEGF-A in the tumor microenvironment are legitimate targets for metastasis prevention.

Chapter Two

Materials & Methods

Animal Husbandry: Before their initiation, all mouse experiments were submitted for approval to the Institutional Animal Care and Use Committee (IACUC) at the University of Texas-M.D. Anderson Cancer Center. 129/SV mice were fed sterile mouse pellets and acidified water ad libitum. Mice were housed in ventilated cages equipped with micro-isolator lids and maintained under strict containment protocols. Evidence of bacterial, parasitic, or fungal infection was tested, and serology was performed on cage littermates for 12 of the most common murine viruses. All mice were euthanized according to the standards set forth by the IACUC.

Antibodies and Recombinant Peptides: We purchased Vimentin and a-SMA for immunocytochemistry staining of primary cells. Sheep anti-Rat Magnetic Dynabeads beads (Invitrogen) were purchased and conjugated to rat anti-mouse antibodies: CD68 (Abcam), CD326 (BD Pharmigen), CD90 (BD Pharmigen and Abcam), CD31 (BD Pharmigen), and F4/80 (AbD Serotec and Abcam) for isolation of the various primary cells from the lungs. Western blot analysis and immunofluoresence experiments were performed using anti-Thy1 (Abcam), anti-FSP1 (Abcam), anti-VEGFR1 (R & D Systems), and anti-VEGFR3 (Santa Cruz Biotechnology) antibodies. For VEGF neutralization and treatment studies, the cells were treated with VEGF neutralizing antibodies, control IgG, or recombinant murine VEGF (R&D Systems), and Avastin (Bevacizumab, Genentech/Roche) provided by M.D. Anderson Cancer Center Pharmacy. For flow cytometry and FACs analysis anti-Thy1-APC (BD

Pharmigen), 7AAD Viability Control (Sigma Aldrich), and anti-CD45-APC (Abcam) antibodies were purchased for cell surfacing staining and sorting.

Cell Lines: The culture conditions and derivation of the cell lines used in this study (LKR-13, MLg, 344SQ, 393P) have been described previously (Gibbons et al., 2009a; Gibbons et al., 2009b; Wislez et al., 2006; Yoshikura and Hirokawa, 1974). The Tyler Jacks group gave us the LKR-13 cells (Massachusetts Institute of Technology), and we purchased the MLg from American Type Culture Collection.

Colony Formation: We formed the cell colonies according to the instructions previously published (Roybal et al., 2011; Zhong et al., 2008). Cells (5×10^4 in 0.3% agar) were seeded onto a layer of 0.8% agar in 6-well plates in normal culture medium, allowed to proliferate for 21 days, and stained with 0.5 mg/mL nitrotetrazolium blue (Sigma-Aldrich). Colonies were visualized by light microscopy (4x) and counted. Results were expressed as the mean ± standard deviation and subjected to the Students t-test for statistical significance.

Cytokine Quantification in Conditioned-Medium: We quantified the secreted soluble factors in the mono- or co-culture conditioned medmium using previously published methods (Roybal et al., 2011). We collected triplicate conditioned-medium samples from three independent migration assay experiments and subjected the samples (n=9) to Magnetic Bead Luminex Pro

Assays according to the manufacturer's instructions. We calibrated each

cytokine using a calibration curve ranging from 2.0 to 32,000pg/mL. We used

the Bio-Plex 2000 Workstation and Bio-Plex Manager (Version 5) software to

acquire and analyze the data. The mean values were calculated from the

replicates and subjected to the Dunnett's Statistical Test to determine

significance between mono-cultures and co-cultures.

FLT1 Transfection shRNA: We performed the FLT1 Transfection shRNA using

a previously published method (Roybal et al., 2011). HuSH™ shRNA plasmid

panels (29-mer) shRNA constructs against Mus Musculus FLT1 in pGFP-V-RS

Vector (TG514364) and Scramble shRNA as the control were purchased

(TR30013) in the pGFP-V-RS plasmid (Origene). The following shRNAmir

sequences were used to create 2 VEGF clones: 5'-

GAAACCACAGCAGGAAGACGGTCCTATCG-3' and 5'-

TGAAGCGGTTCACCTGGACTGAGACCAAG-3'. Constructs were cloned into

competent cells and plated on LB agar containing kanamycin for selection. We

removed single colonies from the antibiotic-treated LB agar plates for each

shRNA construct and scramble control and isolated plasmid DNA for enzyme

digestion. After identifying the clones with the shRNA cassette or scramble

cassette, 344SQ cells were transfected with shRNA or scramble using

lipofectamine and Opti-MEM for 24 hours in an incubator kept at 37°C at 5%

CO_2. Transfection media and reagents were washed with PBS 24 hours after

transfection and replaced with selection media, puromycin (Invitrogen) in

RPMI1640 10%FBS (15μg/mL), for selecting clones. Cells were selected for two weeks to generate stable shRNA populations. Each of the individual clones were chosen from the population of selected cells, tested, and used for various experiments.

Flow Cytometry: We performed flow cytometry using a procedure similar to that in a previously published work (McQualter et al., 2009). Briefly, 129/SV mice were sacrificed according to the regulations set forth by IACUC and UT M.D. Anderson using CO_2 and cervical dislocation. We isolated the lungs from the mice after an intra-tracheal perfusion of HBSS containing 10% FBS (HBSS-10%). To dissociate the lungs into a single cell suspension, we used both an enzymatic digestion with 3mg/mL Collagenase and 4mg/mL Dispase (Roche) and also a lung-specific mechanical technique, the gentleMacs Dissociator (Miltenyi Biotec) programs Lung_0.1 and Lung_0.2. The cell suspension was placed into a red blood cell lysis buffer (Bio Legend), neutralized and centrifuged, resuspended in HBSS-10%, and passed through 70 and 40 micron filters to generate a single cell suspension. Cells were stained with 7AAD, anti-Thy1-APC, and anti-CD45-APC antibodies for one hour, centrifuged, washed, centrifuged, resuspended in 1mL of flow buffer (PBS containing 2% FBS), and counted. Flow cytometric analysis was performed using a fluorescence-activated cell-sorter (FACSDiVA; BD Biosciences), and we analyzed the data collected with FlowJo Software.

Invasion Assay: We performed an invasion assay using a previously published method (Roybal et al., 2011; Zhong et al., 2008). Growth Factor Reduced Matrigel Invasion chambers (BD BioCoat™) was purchased. The upper chamber of the 24-well transwell invasion plate was rehydrated with 500 ul of warm serum-free containing medium and placed at 37°C at 5% CO_2 for two hours. After rehydration, the serum-free containing medium was removed from the upper chambers, and the cells were trypsinized, neutralized with their normal medium containing 10% FBS, spun down, resuspended in serum-free media, counted using a hemocytometer, and placed in the upper chamber at a seeding density of 5 X 10^4 cells per well. The upper chamber containing cells was placed into the lower chamber containing media with 2% FBS at a volume of 600ul/well to act as a chemoattractant. Cells were allowed to invade through the chamber for 14 hours at 37°C at 5% CO_2. The cells on the upper chamber were fixed with 90% ethanol, stained with 0.1% crystal violet blue solution, and rinsed in de-ionized water. The inner portion of the top chamber was swabbed to remove all the non-invaded cells. Migrated cells were counted in five microscopic fields at 4x magnification, which was represented as the mean ± standard deviation and subjected to Students t-test for statistical significance.

Lethal Irradiation and Bone Marrow Engraftment: Total-body irradiation (TBI) was performed with a 137Cs irradiator (Mark I-30; GE), and a single dose of 1000R was given to the recipient animals. Bone Marrow (BM) cells were harvested from femurs and tibias of donor mice. The BM cells were subjected to

T cell-depletion using Miltenyi beads. The adoptive transfer of total BM cells was performed 20-24 hours after TBI via tail-vein injection. For the first two weeks after the TBI/BMT transfer, we prevented infections by giving the recipient mice drinking water supplemented with 25 mg/L neomycin and 13 mg/L polymyxin B sulfate (or Baytril). After week six, blood samples were collected from the tails of Bone Marrow Transfer mice for FACS analysis to check for hematopoietic cell reconstitution. CD11b/Gr-1 staining was used for myeloid cells, CD19/B220 for B cells, and CD3/CD4/CD8 for T cells. In general, more than 90% of hematopoietic cells should be derived from the donor, and those mice were used for orthotopic injections.

Migration Assay: We performed a migration assay according to a previously published method (Zhong et al., 2008). Cells were trypsinized, spun down at 400G for five minutes, and neutralized with their normal medium containing 10% FBS. Cells were then washed with PBS, spun down, resuspended in serum-free media, counted under the microscope using a hemocytometer and trypan blue staining to determine cell viability, and seeded at a density of 5 X 10^4 cells per well into the 0.1% Gelatin pre-coated upper chamber of the 24-well Transwell migration plates (BD Biosciences). The upper chamber containing cells were placed into the lower chamber containing media with 2% FBS at a volume of 600ul/well to act as a chemoattractant. The cells were allowed to migrate through the chamber for 14 hours at 37°C at 5% CO_2. The cells on the upper chamber were fixed with 90% ethanol, stained with 0.1% crystal violet

blue solution, and rinsed in de-ionized water. The inner portion of the top chamber was swabbed to remove all the non-migrated cells. Migrated cells were counted in five microscopic fields at 4x magnification, represented as the mean ± standard deviation and subjected to Students t-test for statistical significance.

Mouse and Cell Genotyping: Genomic DNA from cells was isolated using the Qiagen Genomic DNA Isolation Kit according to the manufacturer's instructions. Genomic DNA was amplified to identify the 393bp band using the following chemical master mix: Water, 10X buffer, 10mM Primers (Kras-Forward Primer 5' – TCACTGAATTCGGAATATCTTAGAG – 3'; Kras-Reverse Primer 5' – GTTTAAAGCCTTGGAACTAAAGGAC – 3'), 10mM dNTPs, Genomic DNA, and Amplitaq (5 units/uL). Genomic DNA was amplified in an Applied Biosystems GeneAmp 9700 PCR Machine with the following program settings for a total of 35 times: 94°C for 5 minutes, 94°C for 1 minute, 56°C for 1 minute, 72°C for 4 minutes, and 72°C for 5 minutes with a final hold at 4°C. Amplified DNA was placed on a 2% Agarose-ETBR-stained gel with a molecular weight marker. Photos were taken of the agarose gel under UV light.

Primary Fibroblast Isolation: We isolated primary fibroblasts using a previously published method (Roybal et al., 2011; Porter et al., 2003). Prior to experimentation, sheep anti-rat Dynal-Invitrogen Magnetic Dyna-beads were washed and conjugated with single rat anti-mouse antibodies (Cocktail)

targeted for different cell-type receptors and left overnight on a rotator at 4°C.

Primary lung fibroblasts or cancer-associated fibroblasts were isolated from the

lungs of syngeneic WT 129/SV mice, Kras^{LA1}, and Kras$^{LA1/+}$; p53$^{R172HDG/+}$ mice.

All mice were sacrificed according to the regulations set forth by IACUC and UT

M.D. Anderson using CO_2 and cervical dislocation. Lungs were briefly perfused

with 2% FBS-HBSS by intra-tracheal administration and stored on ice. Lungs

were dispersed into single cell suspension with 3ug/mL of Collagenase and

Dispase®II (Roche) and were warmed to 37°C utilizing the gentleMACS™

Dissociator from Miltenyi Biotec (Bergisch Gladbach, Germany). To produce a

single cell suspension, Miltenyi Biotec programs Lung_01, and Lung_02 were

used; the cells were centrifuged and washed with 2% FBS-HBSS, and then the

red blood cells were lysed with RBC Buffer (BioLegend). Cells were

centrifuged, washed, and passed through 70μm and 40μm filters to create a

single cell suspension. Cells were counted prior to and after every depletion

using the Invitrogen Countess™. Cells were placed in an ice bucket on a rocker

with the pre-washed antibody-conjugated magnetic beads containing the

following antibody-coated beads: CD45 (Leukocytes), CD31 (enodtelial cells),

EPCAM (epithelial), and F4/80 (macrophage). After 45 minutes, the solution

was placed on a magnet for bead/cell isolation (Invitrogen). We collected the

remaining non-bead conjugated cell suspension and further conjugated it with

magnetic beads against Thy-1 to isolate the Thy-1^{Pos} cells, which we removed

from the beads utilizing HBSS-10% containing 0.5% BSA and 2mmol EDTA.

Cells were washed with HBSS-10%, resuspended, and plated in Alpha-MEM

Medium (Cell-Gro) containing 20% FBS, sodium pyruvate (GIBCO), glutamine (GIBCO), and 100mg/100 U penicillin-streptomycin (GIBCO).

Primary Fibroblast Matrices: We created Primary Fibroblast Matrices using a previously published method (Roybal et al., 2011; Castello-Cros and Cukierman, 2009). Three-dimensional ECMs were generated from LF or CAFs in cell culture. Cells were plated in 6-well plates precoated with gelatin, crosslinked with glutaraldehyde and ethanolamine, washed with PBS, and allowed to adhere at 37°C in 5% CO_2 conditions.   The ECMs to be analyzed grew on cover slips in the 6-well plates. Cells were supplemented with MEM 10% FBS and 50ug/mL ascorbic acid and were allowed to grow for 6-8 days to generate an intact ECM. We washed the media with PBS and added Millipore ddH_2O to lyse the fibroblasts. ECMs were kept in PBS + Gibco Pen-Strep and stored in 4°C in sterile conditions. For analysis of the ECMs, coverslipped samples were removed, fixed in Paraformaldehyde, and permeabalized using Triton X-100. Cells were washed with PBS-Tween (PBS-T) and blocked with the M.O.M. Vector Shield IgG Blocking kit for mice (Vector Labs). Samples were incubated with primary antibody for one hour at room temperature then washed with PBS-T. Secondary antibody was added and incubated at room temperature for 30 minutes. Samples were washed with PBS-T and then were mounted on slides using ProLong Gold Anti-fade with Dapi (Invitrogen). To analyze the samples, we used a confocal microscope (or an epifluoresence microscope that can capture along the z-axis). We acquired images for each

color (channel: Krypton/Argon laser with three lines, 488, 568, 647nm for excitation of the labels) and repeated the process at least five times on different locations of each sample.

Proliferation Assay: We performed a proliferation assay according to a previously published method (Roybal et al., 2011). Cells were trypsinized, spun down at 400G for five minutes, neutralized with their normal medium containing 10% FBS, washed with PBS, and placed in serum-free media. Cells were counted under the microscope using a hemocytometer and trypan blue staining to determine cell viability. The cells were placed into media containing 1% FBS serum, and the cell density was adjusted to achieve 3×10^4 cells per well in 100ul of suspension. The cells were allowed to adhere and were incubated at 37°C at 5% CO_2 for time points every 24 hours for six days. Cells were washed with PBS, trypsinized, and recounted using a hemocytometer to determine cell number in eight independent wells per condition. The results are expressed as the mean ± standard deviation and were subjected to Students t-test for statistical significance.

Quantitative Real Time PCR: We performed quantitative real time PCR using a previously published method (Gibbons et al., 2009a; Roybal et al., 2011; Gibbons et al., 2009b). We performed Q-RT-PCR analysis using the ABI 7500 Fast Real Time PCR Machine (Applied Biosystems), and we normalized the results with a comparative method, acknowledging the L32 ribosomal protein

mRNA as the endogenous house-keeping gene. For each reaction, we

generated a standard curve by using serial dilutions of each of the cDNA.

SYBR Green I (Applied Biosystems) was used as the fluorophore of detection.

All experiments were performed in triplicate, and results are expressed as the

mean ± standard deviation and were subjected to Students t-test for statistical

significance. Specific PCR primer sequences for Q-RT-PCR were designed

with the NIH primer design tool (www.ncbi.nlm.nih.gov/tools/primer-blast/). For

the complete list of primers please see Table 1.

Subcutaneous Tumor Model: We injected tumors subcutaneously using a

previously published procedure (Gibbons et al., 2009a; Roybal et al., 2011).

129/SV mice were injected with tumor cells 1 x 10^6 (n=10 per cell line)

subcutaneously in the right flank using RPMI containing 10% fetal bovine serum

as a vehicle. After monitoring the mice daily for six weeks, we sacrificed the

mice and performed necropsies to isolate and weigh the primary tumors and to

count lung tumor metastases. The weight of primary tumors and metastases

are presented as the mean ± standard deviation and were subjected to

Students t-test for statistical significance.

L32	Forward	TGAAGCAGGCATCTGAGGG
	Reverse	CGAAGGTGGAAGAG TGGGAG
E-cadherin	Forward	CCGCGGCGCACTACTGAGTT
	Reverse	AGGCCGGGCAGGAGTCTAGC
N-Cadherin	Forward	TCGAGC ACCCTTCCCCCGAG
	Reverse	GCGGTGCGACAAAGCTTCCG
Vimentin	Forward	CCAGCACTAGCCGCAGCCTC
	Reverse	GGGTCA CATAGGCGCCACCG
LIFR	Forward	CTCTCAGGCCAGAGTTGAGC
	Reverse	GCTGTTCAGTCAGCCCTCTC
CCR2	Forward	TGTCTTCCCTGAATTGAGCC
	Reverse	AAACGCATTAGTGGACAGGG
IL12R	Forward	CGCAATACGTCGTGCGCTGC
	Reverse	CACTCTGACTCCCACGCGCC
CSF1R	Forward	GCTGGTGCGGATTCGAGGGG
	Reverse	TTCGGCGTTAGTGGCCGAGC
TGFβR1	Forward	ACGCGCTGACATCTATGCAA
	Reverse	CGTCGAGCAATTTCCCAGAA
TGFβR2	Forward	GCGCATCGCCAGCACGATCC
	Reverse	TGGGCTTCCATTTCCACATCCGA
CXCR1	Forward	TCCTCCTGCCGCTGCTCACT
	Reverse	CATGCGCAGTGTGAGCCCGT
CXCR2	Forward	CCTCGTGCCGCTGCTCATCA
	Reverse	GGTGCGCAGTGTGAACCCGT
CXCR3	Forward	GGTCGCACTGCTCTGCGTGT
	Reverse	GGGGCAGCAGGAAACCAGCC
CXCR4	Forward	GAGGCGTTTGGTGCTCCGGT
	Reverse	TCGGTTCCATGGCAACACTCGC
VEGFR1(Flt1)	Forward	CGCGTGAAGAGTGGGTCCT
	Reverse	CACATGCACGGAGGTGTTG
VEGFR2(Flk1)	Forward	AGCCCAGACTGTGTCCCGCA
	Reverse	GGTGTCCGCGGAATCGGGTC
VEGFR3(Flt4)	Forward	GCCCGAGGACGAGGGTGACT
	Reverse	CCTGGCTGCGCCTATCCTGC
human Flt1	Forward	GCACGTCAGCGAAGGCAAGC
	Reverse	CCAGCTCAGCGTGGTCGTAGG

Table 1: Primer sequences used in RT-PCR analysis

Orthotopic Tumor Model: The procedure was followed as previously published, with slight modification (Porter et al., 2003). 129/SV mice (n=10 per cell line) were swabbed with 70% ethanol on their left side in close proximity to the rib cage. The mice were anesthetized using ketamine/xylazine (40 mg/kg) by an intraperitoneal injection. A 20mm incision was made along the left side of the mouse, exposing the rib cage. 344SQ cells were injected in a 1:10 dilution of Growth Factor Reduced Matrigel (BD Biosceinces) to PBS at a seeding density of 2×10^4 cells per 50ml of total suspension per left lobe of the mouse lungs. The skin at the surgical site was then closed with surgical staples and the mice were allowed to recover from the anesthesia. The mice were monitored daily for three weeks and then were sacrificed, necropsied for tumor burden, and examined for visible metastasis. The weight of both the primary tumors and the lungs that showed visible metastasis are presented as the mean ± standard deviation and were subjected to Students t-test for statistical significance.

3' UTR Assays: We performed the *3'*-UTR assays according to a previously published method (Roybal et al., 2011). The 2.0kb Flt1 *3'*-UTR was isolated from a mouse BAC clone by polymerase chain reaction and ligated into the pCI-neo-hRL vector. The 1.9kb *ZEB1* 3'-UTR was subcloned into the same vector and was used as a control for these experiments. The generated reporter constructs were cotransfected with the various miR-200 precursors (5 nmol/L, Ambion) into 24 well plates containing 1×10^5 344SQ cells per well. Using the

Dual Luciferase Reporter Assay (Promega) the luciferase activity was measured after 48 hours post-transfection according to the manufacturer's protocol. We employed a PCR-based site-directed mutagenesis strategy to construct the miR-200 binding site mutants using the following primers (the mutations are highlighted: (mut1) 5'-CCAGCCCCTGACAG<u>GA</u>C<u></u>TATACATCTATGAG-3' and (mut2) 5'-GGTTTTATCTCAAG<u>GA</u>C<u></u>TAATATATAGACAA-3'.

Western Immunoblot: We performed a western immunoblot according to a previously published method (Roybal et al., 2011; Zhong et al., 2008). We isolated cell lysates with a RIPA buffer and quantified the protein witha Pierces BCA Kit. Protein (35μg) was separated on a SDS-PAGE Gel and transferred onto a polyvinylidene fluoride nitrocellulose membrane (Bio-Rad Laboratories). Membranes were blocked over night in 5% milk in TBST at 4°C and washed 3X for 10 minutes in TBST. Primary antibodies were added to 2.5% milk in TBST and applied to the membrane for overnight incubation at 4°C and then washed 6X for 5 minutes in TBST. Secondary antibodies were added to 1% milk in TBST, allowed to incubate at room temperature for two hours, and then washed 3X for 10 minutes. Antibody binding was detected with an enhanced chemiluminescence kit according to the manufacturer's instructions (Amersham).

Chapter Three

Results

Carcinoma-Associated Fibroblasts are biochemically and morphologically different from normal lung fibroblasts.

We must fully understand not only the pathophysiological context of the disease but also the molecular and cellular events within the entire microenvironment. To further elucidate the stromal contribution to the cancer process within the lung tumor microenvironment, we chose to study cancer-associated fibroblasts (CAF) in metastatic lung cancer disease. While several studies of various cancers have shown that CAF promotes angiogenesis, tumor cell proliferation, and tumor progression, no other studies, to our knowledge, have demonstrated this correlation in metastatic lung cancer (Liao et al., 2009; Zhang et al., 2011; Zeine et al., 2009). To that end we used tumor cell lines from a murine lung cancer model that develop lung adenocarcinomas with a defined metastatic potential through the expression of two specific mutations: the first is a common Li-Fraumeni Tp53 mutation ($p53^{R172H_\Delta G/+}$) found in Li-Fraumeni patients and the second a $Kras^{LA1/+}$ ($K\text{-}ras^{G12D}$) mutation (Figure 3A and Figure 3B)(Gibbons et al., 2009a; Roybal et al., 2011). Lung tissues from K-ras, K-ras p53, and wildtype 129/SV syngeneic mice were enzymatically digested with collagenase and dispase into a single cell suspension. We used a magnetic bead approach to acquire CAF from the lungs of mice that express a somatic recombination of the latent K-ras (K-rasG12D) mutant allele, CAFp53 from Kras;p53 mice, and Lung Fibroblasts (LF) from syngeneic 129/SV wildtype litermates (Schematically shown in Figure 4)(Johnson et al., 2001). To remove

A

Experimental Metastasis Model

$Kras^{G12D/+}$

Lung adenocarcinoma
(no metastases)

$Kras^{G12D/+}$ $p53^{R172H/+}$
Li-Fraumeni mutation

Metastatic disease

B

Cell Lines
- 344P, LN, SQ
- 393P, LN

SQ Injection

$Kras^{G12D/+}$ $p53^{R172H/+}$

Syngeneic WT mice
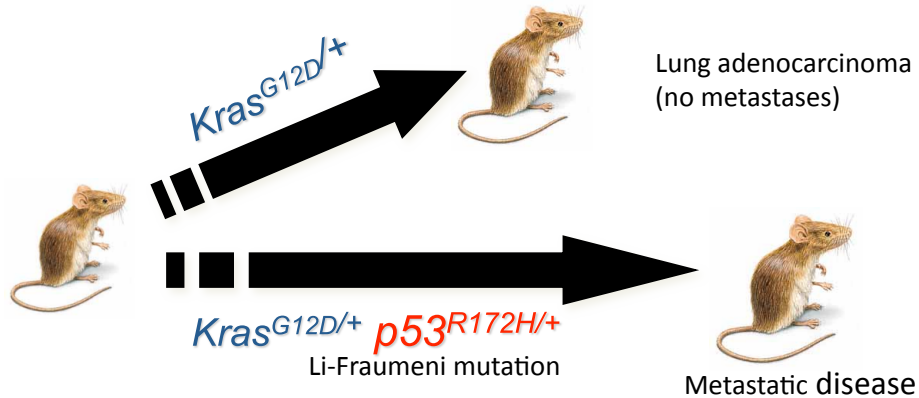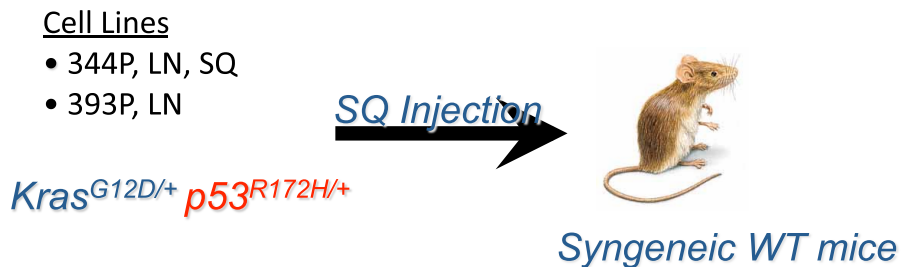
	Route of Injection	Local	Metastasis	Metastatic Sites
393 Primary	SQ	7/10	**0/10**	None
393 LN Met	SQ	6/6	**0/6**	None
344 SQ Met	SQ	13/13	**13/13**	lung, pancreas, adrenal, muscles, diaphragm, bone

Figure 3: Murine Lung Cancer Models.
(A) Schematic representation of the two mouse models ($Kras^{LA1/+}$ and $Kras^{LA1/+}$; $p53^{R172H\Delta G/+}$ mice) used. $Kras^{LA1/+}$ mice have a spontaneous recombination of the Kras G12D allele and develop lung adenocarcinomas that do not metastasize. $Kras^{LA1/+}$; $p53^{R172H\Delta G/+}$ have both the Kras and p53 mutation that undergo spontaneous recombination to produce metastatic lung adenocarcinomas. **(B)** Cell lines isolated from $Kras^{LA1/+}$; $p53^{R172H\Delta G/+}$ mice have different metastatic potentials. Cells were taken from various sites of metastases and injected subcutaneously into wildtype 129/SV mice. Six weeks post-injection, mice were sacrificed and metastases were quantified. These results have been previously published (Gibbons 2009). Figure kindly provided and adapted from Don. L Gibbons, M.D., Ph.D.
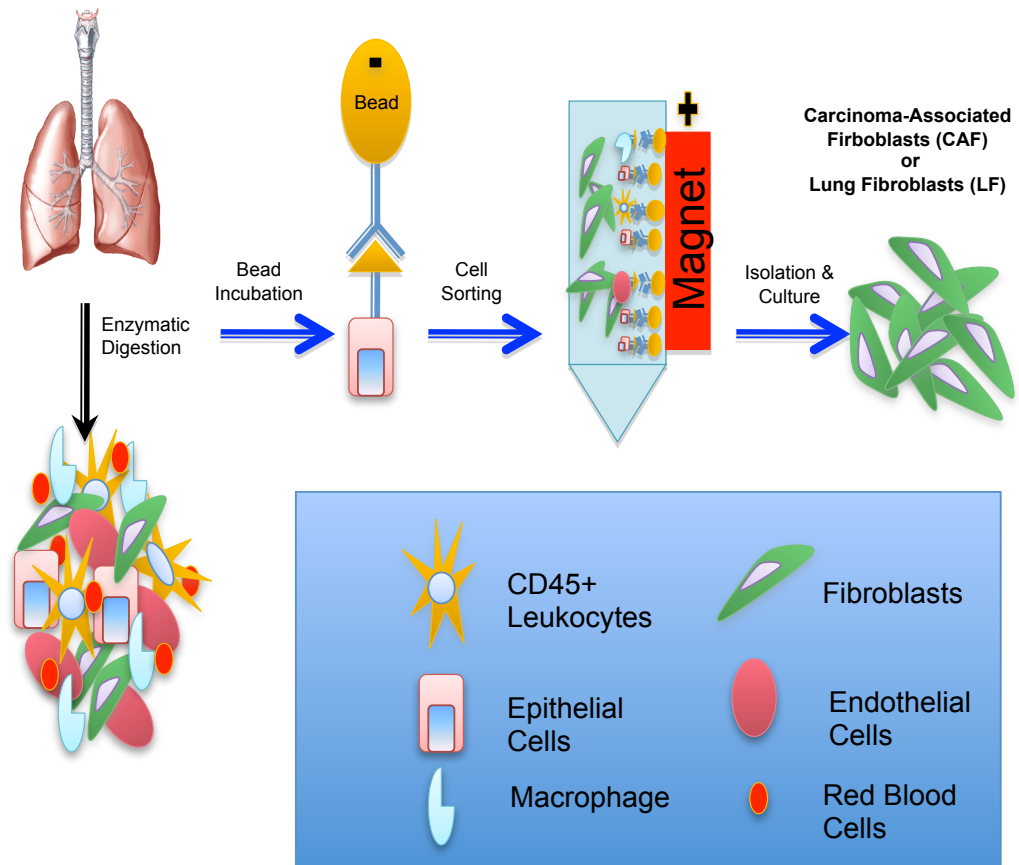
Figure 4: Primary Cell Isolation Technique.

Lungs isolated from Kras[LA1], Kras;p53, and wildtype129/SV mice littermates were mechanically (Mylteni gentleMACS DIssociator Lung Program 1 and 2) and enzymatically digested with Collagenase and Dispase to acquire a single-cell suspension. The suspension was then incubated with Dynal magnetic beads that had been conjugated to various antibodies that recognize particular cell surface receptors for certain cell types. After 30 minutes of incubation with the beads the cell suspension was placed on a magnet to remove the unwanted cells and to acquire the cells of interest.

all the unwanted cells from the cell suspension, we used a negative selection method: antibody-conjugated magnetic beads attracted endothelial cells (CD31), leukocytes (CD45 and CD68), macrophage (f4/80), and epithelial cells (EP-CAM)(Figure 3). To positively select for fibroblasts, we combined the remaining cell suspension with magnetic beads conjugated to Thy1^{Pos} (CD90), a glycosylated cell surface protein expressed on lung fibroblasts, thymocytes, inflammatory cells, peripheral T cells, and neuronal cells (Rege and Hagood, 2006). To validate the purity of the cells we performed quantitative real-time PCR and western blot analysis on isolated cells, which revealed Thy1^{Pos} fibroblasts cells were negative for leukocyte, macrophage, epithelial, and endothelial cell surface markers (Figure 5A) and expressed common fibroblast markers such as Thy1 and Fibroblast Specific Protein 1(FSP-1)(Figure 5B). After culturing, the isolated CAF and LF displayed clear morphological differences: CAF were more rounded and smaller with fewer cellular projections, whereas LF were more flat and showed heavy branching (Figure 5C). In addition to their morphological differences, CAF proliferated more rapidly (Figure 5D), expressed higher levels of α-SMA (Figure 5E), and had stress fibers arranged in parallel sheets, whereas LF had stress fibers that were interwoven (Figure 5F). Cells isolated by the same approach from the lungs of Kras$^{LA1/+}$; p53$^{R172H_{\Delta}G/+}$ mice (CAFp53) expressed α-SMA and vimentin and were morphologically indistinguishable from CAF derived from Kras^{LA1} mice (Figure 5F). To corroborate our *in vitro* studies, we performed in situ staining of α-SMA on three lung adenocarcinoma patient samples, which revealed positive
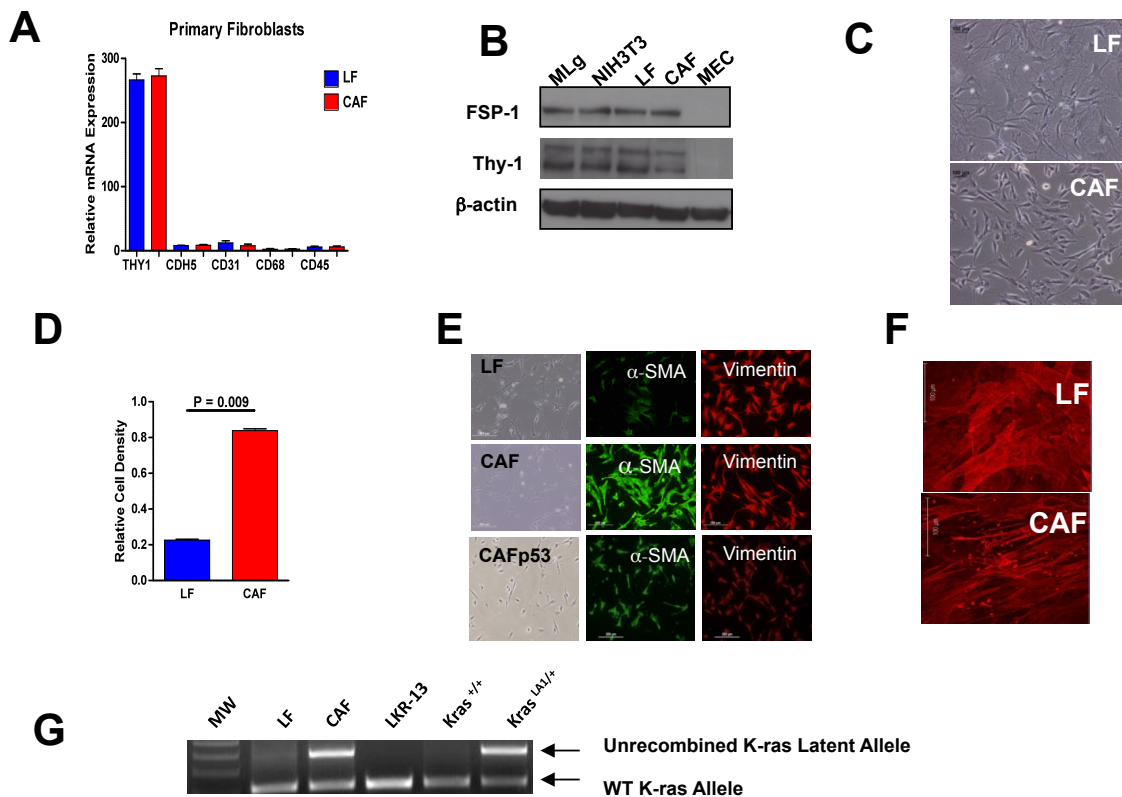
Figure 5: Characterization of LF and CAF.
(A) Primary fibroblasts only express the fibroblast's marker Thy1. Quantitative RT-PCR analysis of LFs. Values normalized on the basis of L32 ribosomal protein mRNA levels. **(B)** Primary fibroblasts express common fibroblast protein markers. Western blotting of fibroblast-specific protein-1 (FSP-1) and Thy-1 (1.1 and 1.2 alleles expressed as two distinct bands) in LFs and CAFs. Positive (MLg and NIH3T3) and negative (MEC) controls indicated. β-actin used as a loading control. **(C)** LF and CAF are morphologically different from each other. Morphology of primary lung fibroblasts (light microscopic images at 20x magnification). Bar indicates 100 μm. **(D)** CAF proliferate faster than LF. LF and CAF were seeded at a density of 3.0 X10^4 and proliferative rate measured with WST-1 Reagent after 72 hours. **(E)** CAF and CAFp53 exhibit an activated myofibroblast phenotype. Detection of fibroblast markers in LFs, CAFs, and CAFp53 by immunocytochemistry imaged by fluorescent or light microscopic analysis (20x magnification) of identical fields. Bar indicates 200 μm. **(F)** Distinct patterns of stress fibers in LFs and CAFs. Immunofluorescent staining and laser scanning confocal imaging of α-smooth muscle actin in 3-D matrices produced by fibroblasts after extraction of cellular debris. Bar indicates 100 μm. **(G)** No evidence of genetic recombination of the latent *K-ras* allele in CAF. PCR amplification of *K-ras* alleles from genomic DNA use primers that distinguish wild-type (bottom arrow) from unrecombined mutant allele (top arrow) on the basis of product size; the product generated from the recombined mutant allele is the same size as that of the wild-type allele (bottom arrow). Recombination leads to loss of top band. Controls include LKR-13 (lung adenocarcinoma cells with recombined Kras^{LA1} allele) and tail clips from wild-type mice (Kras$^{+/+}$) and Kras$^{LA1/+}$ mice (heterozygous for Kras^{LA1} allele). Adapted and reprinted by permission from the American Association for Cancer Research: J.D. Roybal, Y. Zang, and Y.-H, et al., miR-200 Inhibits Lung Adenocarcinoma Cell Invasion and Metastasis by Targeting *Flt1/VEGFR1*, *Mol Cancer Res*, 2010, (9);25, 25-35.

staining within the tumors (Figure 6). Although these features are consistent

with those of fibroblasts isolated from both tumors and matched normal tissues,

these differences might be explained by the fact that CAF underwent a somatic

recombination of the latent K-rasG12D allele, which was excluded by analysis

of genomic DNA (Figure 5G)(Desmouliere et al., 2004).

From the above findings we sought to quantify the abundance of Thy1^{Pos}

fibroblasts within the Kras^{LA1} mice and the wildtype littermates. The same

antibody clones used for fibroblast isolation were fluorescently labeled and

applied to dispersed lung cells for flow cytometric analysis that quantified

Thy1^{Pos} lung fibroblasts in KrasLA1 mice and wildtype littermates (n=5 for each)

(Figure 7A) Thy1^{Pos} lung fibroblasts (CD45^{Neg}, CD31^{Neg}, EpCAM^{Neg}, and

Thy1^{Pos}) constituted a significantly higher proportion of the total dispersed lung

cell population in Kras^{LA1} mice than they did in wildtype mice (4.97 ± 0.61%

versus 3.03 ± 0.28%, respectively, p=0.02, Figure 7B) and were three-fold more

abundant in Kras^{LA1} mice than they were in wildtype mice (82,564 ± 22,719

cells *versus* 26,748 ± 5,129 cells per lung, respectively, p=0.04, Figure 7C).

Collectively, these findings from two mouse models of lung adenocarcinoma

provide evidence of a Thy1^{Pos} CAF population that is morphologically and

biochemically distinct from its normal tissue counterpart and is more abundant

in the lungs of tumor-bearing Kras^{LA1} mice.
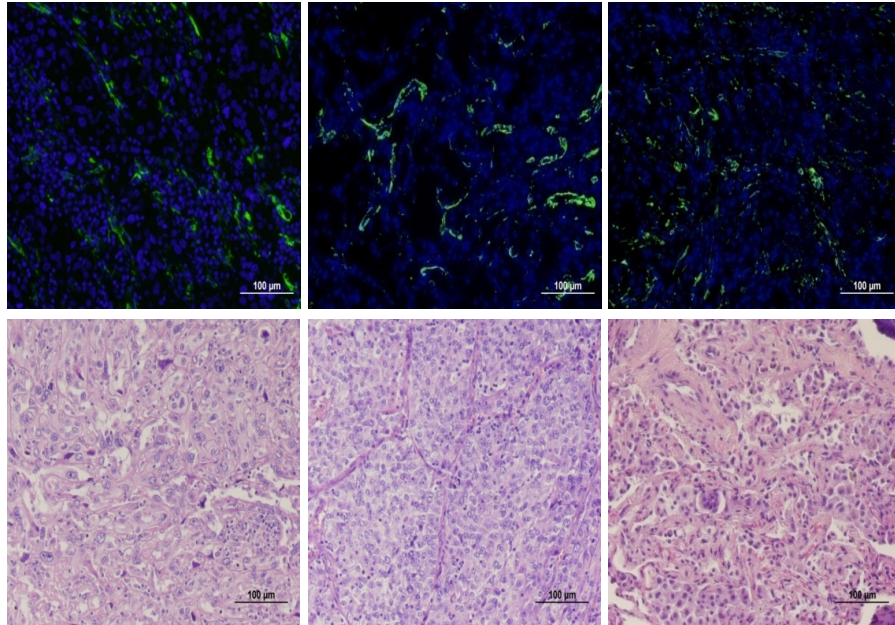
Figure 6: Intratumoral α-SMA expression in human lung adenocarcinomas.
Lung adenocarcinoma patient samples stain positive for the myofibroblast marker α-SMA. Lung adenocarcinomas from three patients were stained with anti-α-SMA antibodies, which were detected by immunofluorescent staining (green). Adjacent tissue sections were stained with hematoxylin and eosin.
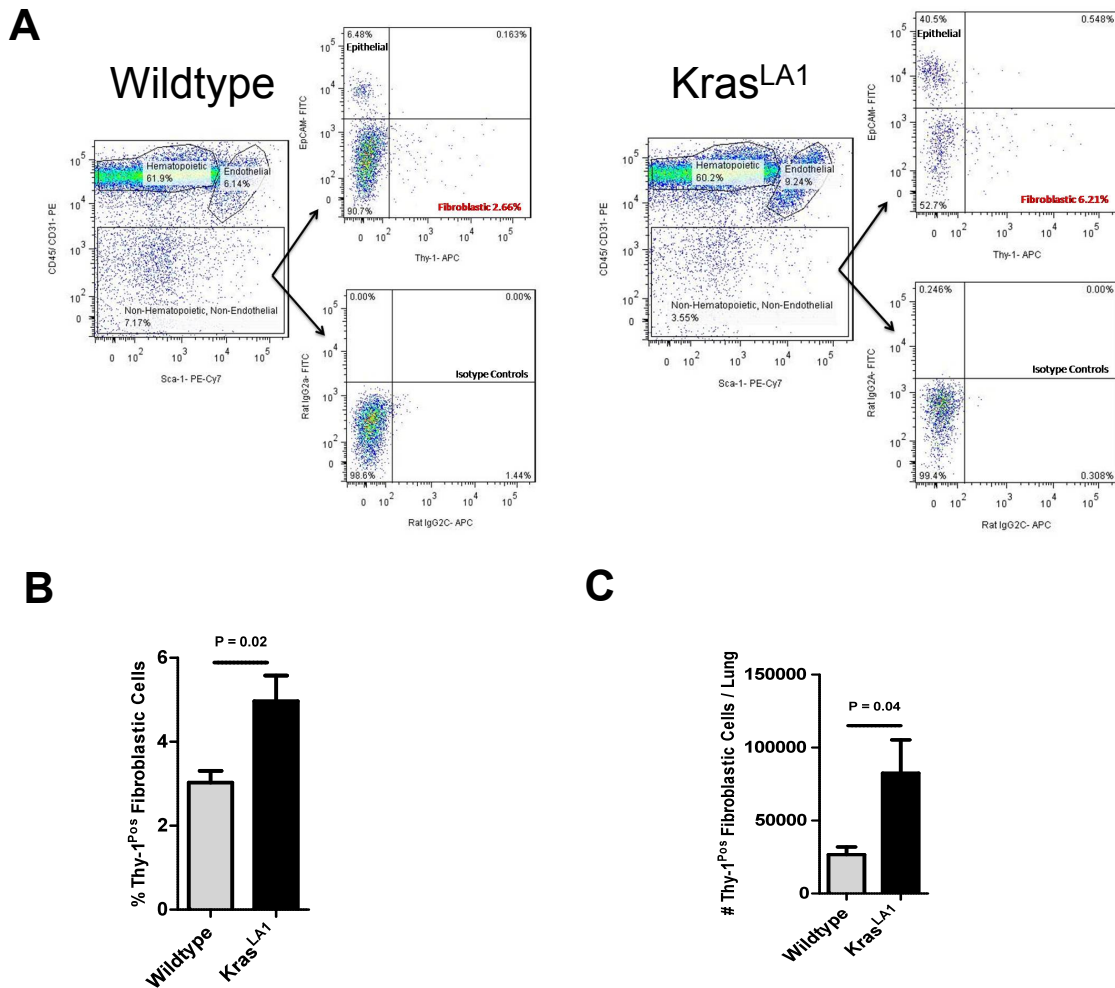
Figure 7: Relative abundance of Thy1[Pos] LF and CAF in Kras[La1/+] and wild-type littermates.

(**A**) Strategy used for Kras[LA1/+] and wildtype littermates. Gating strategy used to quantify Thy1^{pos} fibroblasts (Thy1[Pos] CD45[Neg] CD31[Neg] EpCAM[Neg]) by negative selection of hematopoietic cells (CD45[Pos]), endothelial cells (CD31[Pos] Sca-1[Pos]), and epithelial cells (Ep-CAM[Pos]) and positive selection of fibroblasts (Thy1[Pos]). The locations of each cell type within flow plots for wildtype mice (left) and Kras[LA1] mice (right) are indicated. Thy1[Pos] fibroblasts were quantified based on (**B**) the relative frequency within the lung and (**C**) the absolute numbers of cells per lung.

Functional interactions between tumor cells and lung fibroblasts*.*

On the basis of the morphological differences between LF and CAF, the positive staining of α-SMA on CAF demonstrating an activated fibroblast phenotype (Figure 5E), and previous reports of activated fibroblasts having pro-cancerous effects, we postulated that CAF could promote tumor cell invasion to enhance metastasis. We tested for tumor cell invasion *in vitro* by co-culturing 344SQ cells with fibroblasts (LF, CAF, or CAFp53) in a Boyden apparatus, which contains two chambers separated by a porous membrane coated with Matrigel that allows the exchange of soluble factors between the co-cultured cells. 344SQ cells were more invasive in co-culture with CAF or CAFp53 than they were in co-culture with LF (2.1-fold, *P*=0.002, two-sided Student's t-test, Figure 8A). To further corroborate these results, we conducted studies on four other lung adenocarcinoma cell lines derived from Kras$^{LA1/+}$; p53$^{R172H\Delta G/+}$ mice; these results showed an increase of invasion of the cancer cells toward CAF through the invasion chamber (Figure 8B) and tumor cells reciprocally chemoattracted CAF and CAFp53 more prominently than they did LF in the dual-chamber migration assays (Figure 9A). We also conducted studies on two other lung adenocarcinoma cell lines, which showed an increase in the migration of the CAF toward the cancer cells when compared to LF (Figure 9B). On the basis of these findings, syngeneic mice were injected subcutaneously with a lung adenocarcinoma cell line 393P, derived from KrasLA1/+; p53$^{R172H\Delta G/+}$ mice (Gibbons et al., 2009b). Because this cell line has a low tumorigenicity, we tested it both alone and in combination with either CAF or LF
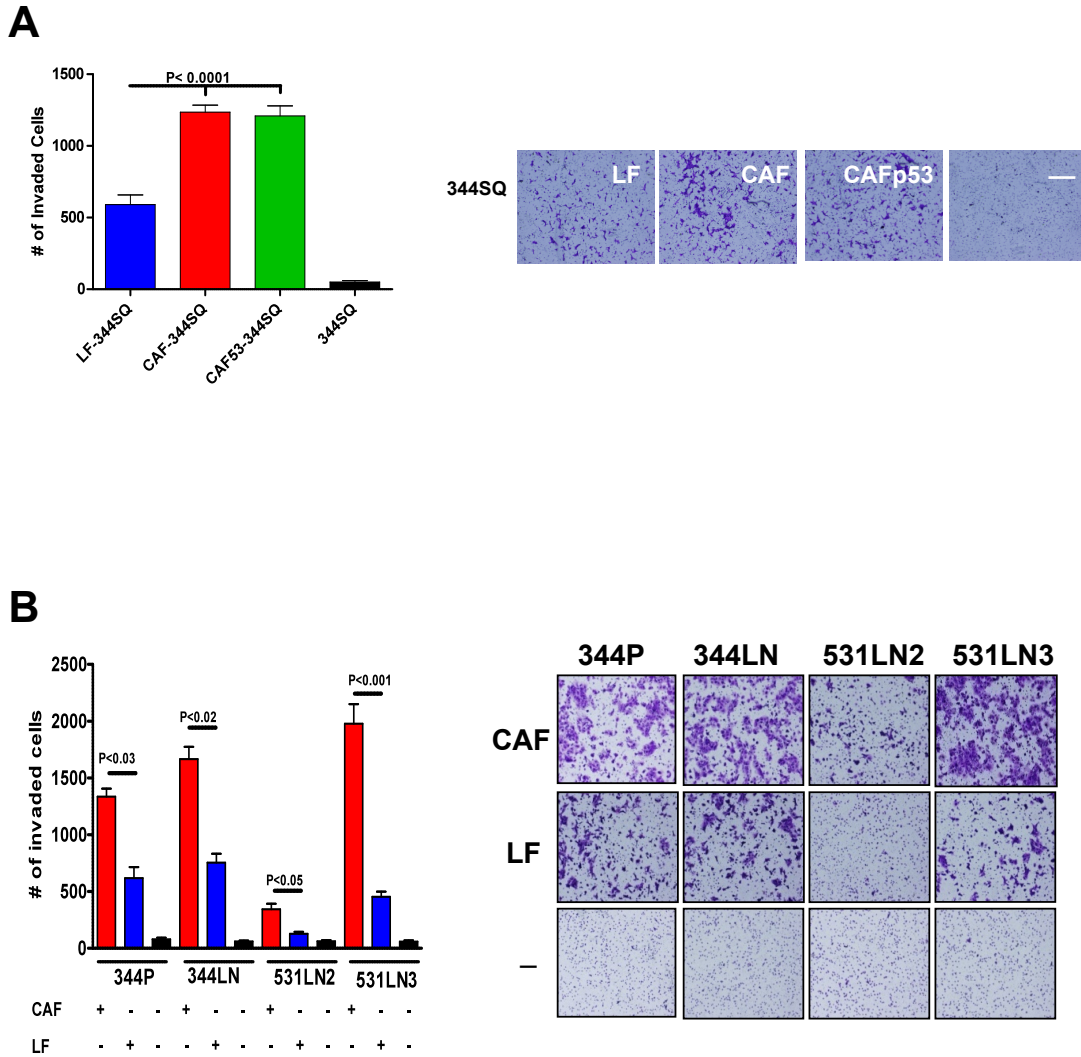
Figure 8: Fibroblast-induced tumor cell invasion.
(A) CAF and CAFp53 induce 344SQ invasion. 344SQ cells were mono-cultured (-) or co-cultured with LF (LF), CAF, or CAFp53 derived from $Kras^{LA1}$ mice (CAF) or $Kras^{LA1/+}$; $p53^{R172H\Delta G/+}$ mice. Invasive tumor cells were photographed (images) and counted in at least 5 separate microscopic fields per well, which were averaged, and the mean values per well ($\pm$ SD) were calculated from replicate wells (bar graphs). **(B)** CAF and CAFp53 induce other tumor cells to invade. Experiment was repeated using other tumor cells (344P, 344LN, 531LN2, and 531LN3) derived from $Kras^{LA1/+}$; $p53^{R172H\Delta G/+}$ mice instead of 344SQ. Adapted and reprinted by permission from the American Association for Cancer Research: J.D. Roybal, Y. Zang, and Y.-H, et al., miR-200 Inhibits Lung Adenocarcinoma Cell Invasion and Metastasis by Targeting *Flt1/VEGFR1*, *Mol Cancer Res*, 2010, (9);25, 25-35.
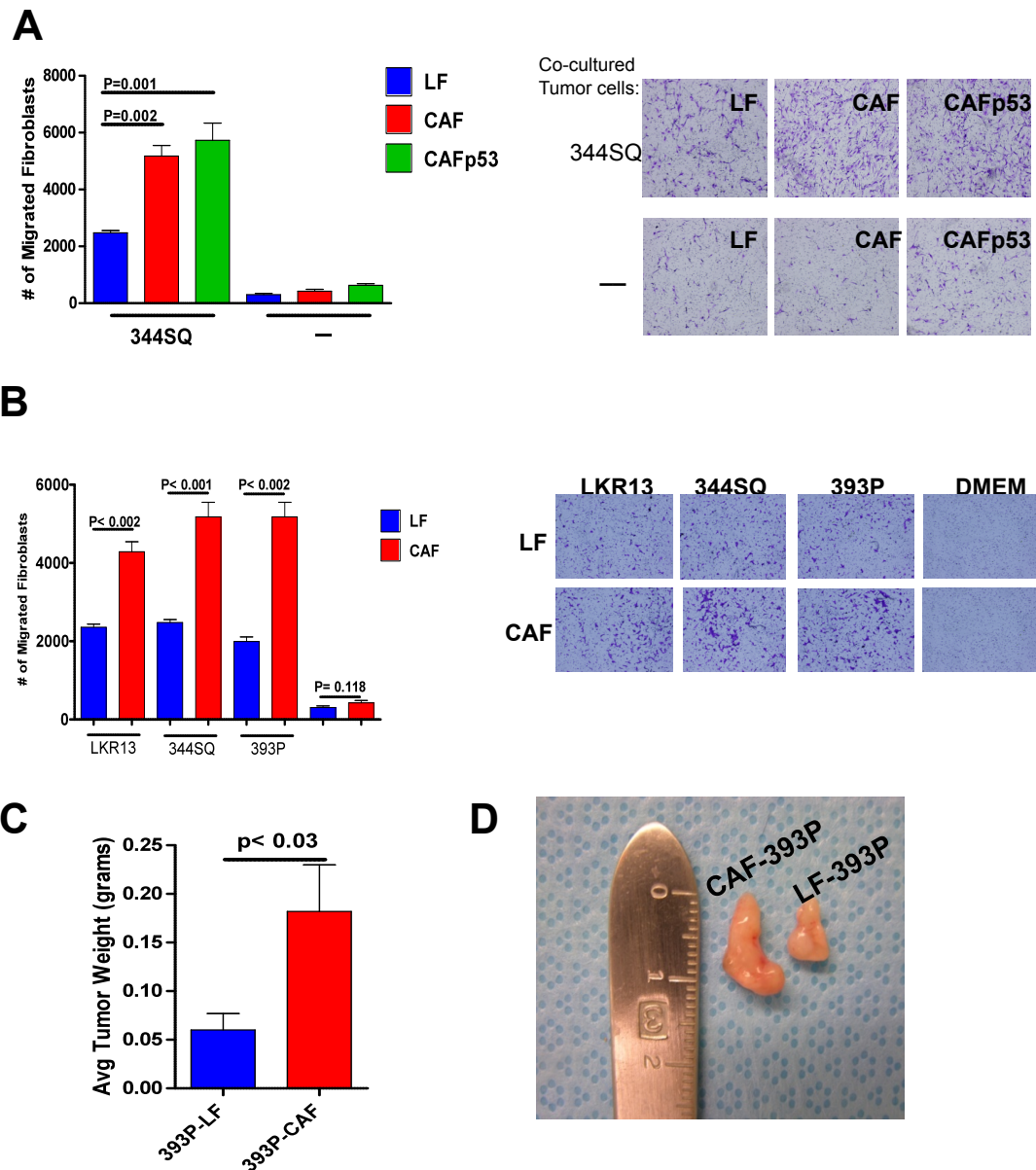
Figure 9: Interactions between tumor cells and lung fibroblasts.
(A) Tumor cell-induced fibroblast migration. Fibroblasts (LF or CAF) were mono-cultured (-) or co-cultured with 344SQ cells. Migrated fibroblasts were counted in at least 5 separate microscopic fields per well, which were averaged, and the mean values per well (± SD) were calculated from replicate wells (bar graphs). Images illustrate representative fields. **(B)** Tumor cell-induced fibroblast migration. Fibroblasts (LF or CAF) were mono-cultured (-) or co-cultured with tumor cells (LKR-13, 344SQ, or 393P). Migration was quantified in the same manner as **A**. **(C)** Fibroblast-induced tumor growth. 393P tumor cells (10^6 per mouse) were injected alone or co-injected with LFs or CAFs (10^6 per mouse) into subcutaneous flank (n=3 mice per cohort). Resulting tumors were isolated, weighed (grams, bar graph), and photographed (image). Tumors that arose in the absence of fibroblast co-injection were too small to measure and are not included.

to determine whether CAF combined with 393P would increase the

tumorigenicity and metastatic potential of the 393P cell line(Gibbons et al.,

2009b). Tumors developed in all 10 mice co-injected with CAF or LF (n=5 mice

for each) and in two of five mice injected with 393P cells alone (P=0.17, Fisher's

exact test). Tumor weight was also significantly greater in mice co-injected with

CAF than in those co-injected with LF (P=0.001, two-sided Student's t-test,

Figure 9C and 9D), which suggests that CAF increase the tumorigenicity of

tumor cells but do not increase the metastatic potential. Collectively, these

findings indicate that lung adenocarcinoma cells have distinct functional

interactions with LF and CAF.

Proteins secreted by tumor cells and lung fibroblasts*.*

Previous reports in the literature and our findings *in vitro* led us to

postulate that CAF and LF have disparate secretomes that account for their

different abilities to induce tumor cell invasion (Mishra et al., 2011). We

collected conditioned media samples from the dual-chamber Boyden migration

assays and quantified the concentrations of a panel of cytokines, chemokines,

and growth factors using BioRad's Luminex Multiplex Magnetic Bead Pro

technology (Figure 8A, n=9 samples per condition). The Luminex Multiplex

antibody-based assay revealed at least a two-fold increase in concentration of

monocyte chemotactic protein-1 (MCP-1/CCL2); the murine functional

homologues of human CXCL1 (KC and MIP2), VEGF-A, interleukin-6; and

others when comparing mono-cultures of CAF to either LF or 344SQ (Table 2).

Proteins	344SQ	LF	CAF	LF/344SQ	CAF/344SQ
MCP-1	9.11	282.46	2524.16	1182.22*	2711.63*
MIP-1α	21.29	21.67	59.85	33.2	177.97*
MIP-1β	0.75	2.71	60.64	14.16*	142.34*
RANTES	0.5	1.22	19.65	9.40*	29.24
Eotaxin	76.12	36.8	149.24	86.01	196.3
KC	486.38	52.69	1191.99	809.42	2370.50*
MIP-2	2.24	3.9	118.74	31.07*	1119.31*
MIG	2.51	1.58	31.82	10.08*	69.44*
bFGF	1.94	2.07	12.57	5.28*	19.08*
PDGF-β	38.86	22.36	17.41	13.67	13.58
VEGF-A	61.94	8.3	409.68	85.75*	712.91*
VEGF-D	0.92	6.33	3.82	0.5	11.75
IL-1α	0.2	0.33	1.71	0.43	1.56
IL-1β	6.87	3.36	23.35	10.15*	34.51*
IL-2	0.75	0.7	1.55	0.69	1.64
IL-3	0.03	0.18	0.24	0.09	0.29
IL-4	0.04	1.67	0.21	0.04	0.27
IL-5	0.41	0.6	1.28	0.49	1.66
IL-6	1.29	30.2	1838.95	128.90*	675
IL-9	5.15	2.35	23.67	4.42	24.96
IL-10	0.87	0.48	2.08	0.85	2.95*
IL-12(p40)	0.43	0.32	1.65	0.54*	2.21*
IL-12(p70)	22.89	22.64	39.19	28.82*	41.69*
IL-13	34.08	27.36	53.69	30.29	61.19
IL-17	0.23	0.34	0.97	0.25	1.22
IL-15	2.38	1.78	40.17	12.2*	76.29*
IL-18	16.02	18.35	55.4	19.44	78.42*
TGF-β1	852.39	110.68	1875.37	903.56*	2687.85*
G-CSF	10.09	3.67	47.43	32.76*	122.32*
GM-CSF	16.37	3.93	12.22	16.21	27.56*
M-CSF	13.29	32.54	106.95	59.80*	132.21*
IFN-γ	3.24	2	8.58	3.48	10.85
TNF-α	7.67	5.82	15.7	8.61	20.92*
LIF	30.62	7.74	103.94	36.23	171.74*

Table 2: Protein concentrations in conditioned media from mono- and co-cultures.

Protein concentrations are pg/ml. Comparisons (co-culture *versus* either of two mono-cultures) were based on Dunnett's test. * indicates protein concentrations that were significantly different (p<0.05) in co-culture relative to that of either of the monocultures. Adapted and reprinted by permission from the American Association for Cancer Research: J.D. Roybal, Y. Zang, and Y.-H, et al., miR-200 Inhibits Lung Adenocarcinoma Cell Invasion and Metastasis by Targeting *Flt1/VEGFR1*, *Mol Cancer Res*, 2010, (9);25, 25-35.

Additionally, several proteins increased sharply in the co-cultures relative to their levels in mono-cultures, including TGFβ1, VEGF-A, monokine induced by interferon-γ (MIG/CXCL9), KC, MIP2, macrophage inflammatory protein (MIP-1α/CCL3), MIP-1β/CCL4, MCP-1, and leukemia inhibitory factor (LIF, Table 2). Moreover, the presence of an activated CAF in the CAF-344SQ co-cultures enhanced the secretion of soluble factors in CAF-344SQ co-cultures when compared to LF-344SQ co-cultures. Of note, we detected VEGF-A (409.68 pg/mL) as one of the most abundant proteins in CAF conditioned media samples, whereas VEGF-D (3.82 pg/mL), a VEGFR3 ligand, is present at extremely low levels.

Given the high concentrations of ligand proteins in the CAF-344SQ co-cultures that might regulate 344SQ cell invasion, we chose to narrow the focus of our investigation to those ligands for which 344SQ cells expressed receptors most prominently. Examination of the mRNA levels of thirteen different receptors in 344SQ cells revealed that VEGFR1 (*Flt1*), VEGFR3 (*Flt4*), and TGFβ type I (*Tgfbr1*) and type II (*Tgfbr2*) receptors were over fifty-fold more abundant than any of the other receptors expressed on 344SQ (Figure 10A). Of note, the high levels of TGFβ receptors are consistent with the reported sensitivity of 344SQ cells to TGFβ1-induced EMT and invasion (Gibbons et al., 2009b). In addition to the mRNA levels, we could readily detect VEGFR1 by western blotting of cultured 344SQ cells (Figure 10B) and by immunofluorescent staining of 344SQ tumors in syngeneic mice (Figure 10C).
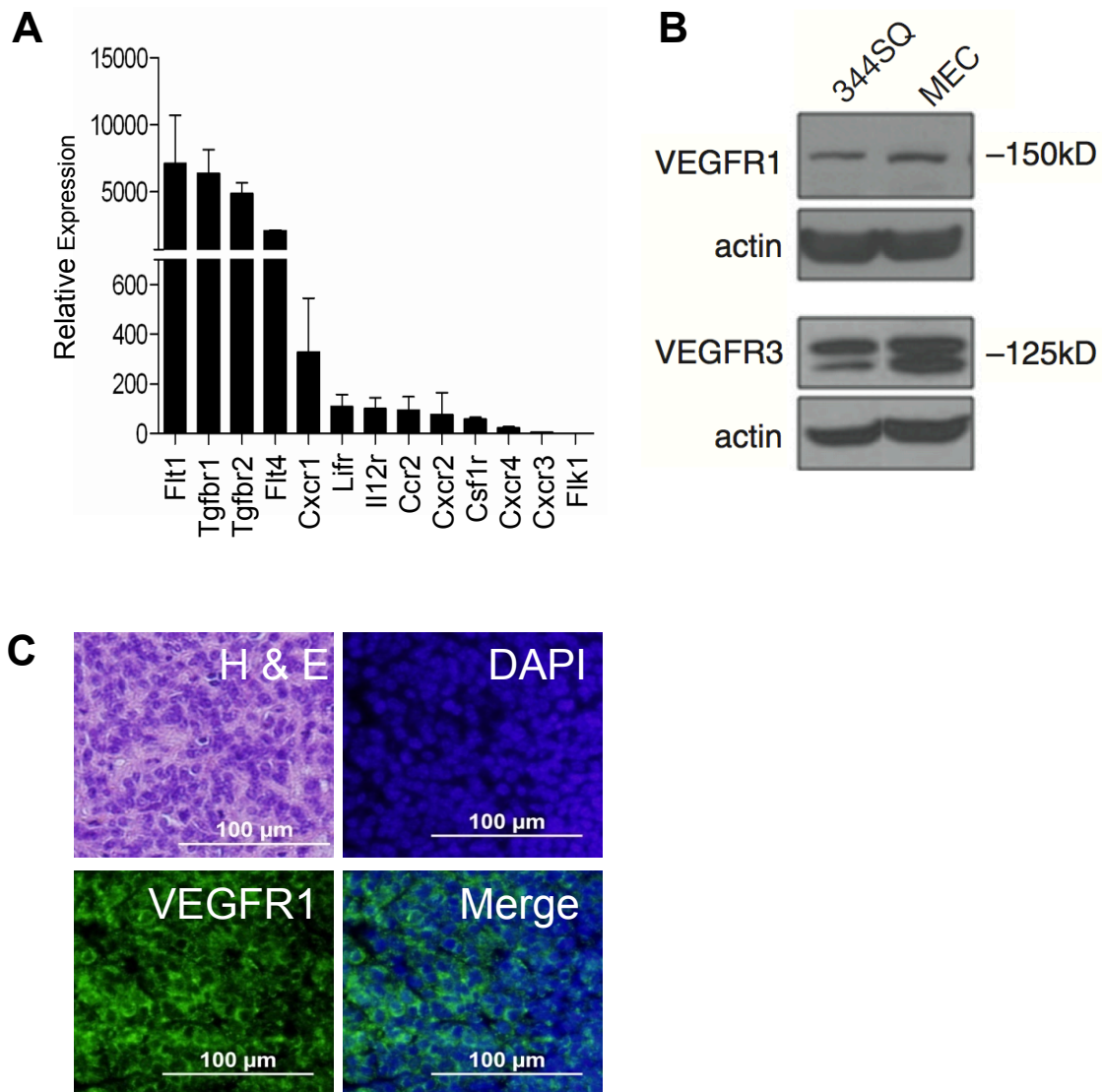
Figure 10: Cytokine receptor expression on 344SQ cells.
(**A**) Relative mRNA levels of 13 different cytokine receptors in 344SQ cells. Quantitative PCR results are the mean values from triplicate samples, which were normalized on the basis of Flk1, set at 1.0. (**B**) Western blotting of 344SQ cells detected VEGFR1 and C-terminal proteolytically cleaved forms of VEGFR3. Murine lung endothelial cells (MEC) included as control. (**C**) VEGFR1 detected in cytoplasmic and plasma membranous compartments. Immunofluorescent staining of a 344SQ syngeneic tumor with anti-VEGFR1 antibody (green) and 4',6-diamidino-2-phenylindole (DAPI, blue) to detect nuclei. Adjacent tissue section stained with hematoxylin and eosin. . Adapted and reprinted by permission from the American Association for Cancer Research: J.D. Roybal, Y. Zang, and Y.-H, et al., miR-200 Inhibits Lung Adenocarcinoma Cell Invasion and Metastasis by Targeting *Flt1/ VEGFR1*, *Mol Cancer Res*, 2010, (9);25, 25-35.

VEGFR1 promotes tumor growth, invasion, and metastasis.

To model the effects of VEGFR1 targeting on tumor cells, we stably

introduced VEGFR1 short hairpin RNA (shRNA) into 344SQ cells. We chose

two 344SQ_VEGFR1 shRNA clones (#2-3 and #4-1) that expressed decreased

VEGFR1 mRNA and protein levels for further study (Figure 11A). The

VEGFR1-depleted tumor cells demonstrated a decrease in proliferation in

monolayer culture (Figure 11B), a decrease in invasion in co-culture with CAF

(Figure 11C), and a decrease in colony formation in soft agar (Figure 11D).

Additionally, when we subcutaneously injected the VEGFR- depleted cells into

syngeneic mice, we saw a decrease in the metastatic potential of these cells

when compared to the scramble control shRNA transfectants (Figure 11E).

Because VEGFR1 is required for tumor growth and metastasis, we

posited that VEGFR1 expression in primary tumors adversely affects the clinical

outcome for lung adenocarcinoma patients. We mined publicly available gene

expression databases for VEGFR1 mRNA expression in resected tumors from

two cohorts of early-stage lung adenocarcinoma patients that are well-

annotated for clinical outcome (Chitale et al., 2009; Tomida et al., 2009). We

grouped and compared the patients on the basis of VEGFR1 expression (top

quartile versus the lower three quartiles) and the duration of survival in the two

groups (Figure 12A). We observed that patients in the top quartile of one cohort

fared worse, having a significantly shorter duration of survival than did those in

the lower three quartiles ($P=0.007$, Log-rank test; $P=0.016$, univariate Cox,

Figure 12A)(Tomida et al., 2009).   We discovered a similar correlation between
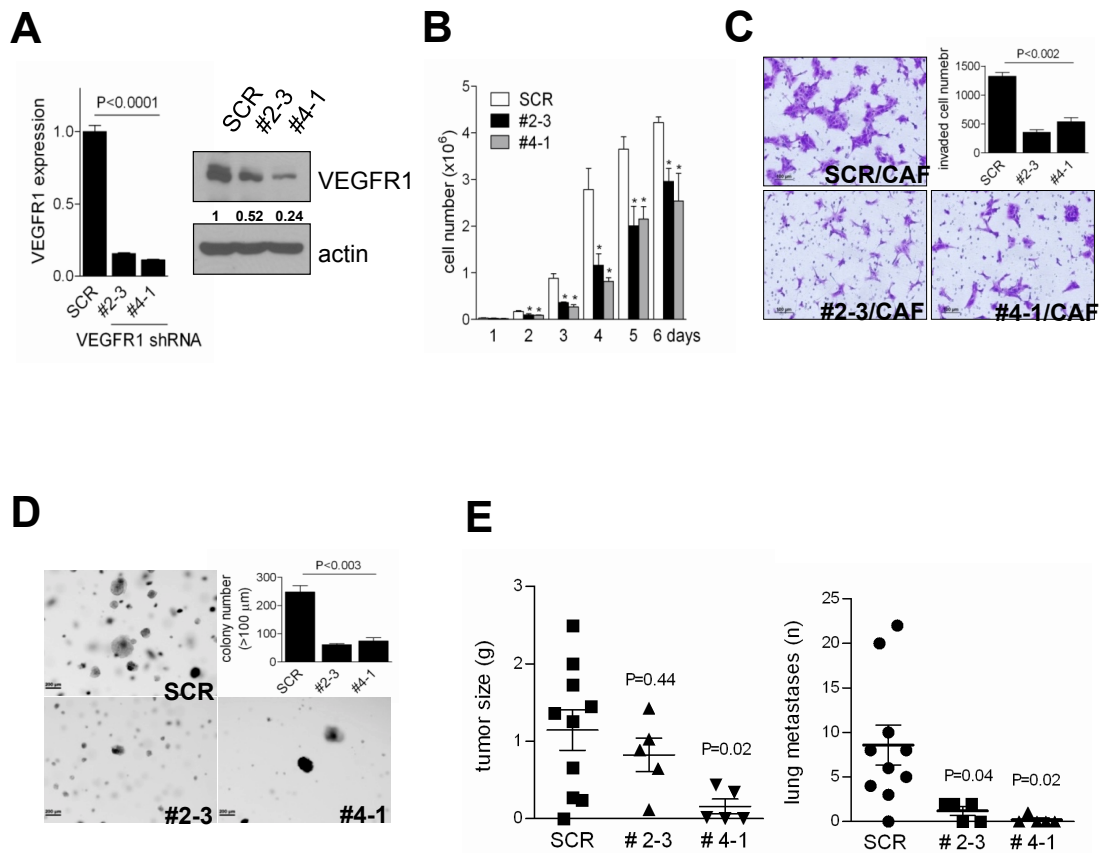
Figure 11: Biologic properties of tumor cells regulated by VEGFR1.
(**A**) Suppression of VEGFR1 by VEGFR1 shRNA. Quantification of VEGFR1 in two independent clones of 344SQ transfected with VEGFR1 shRNA (#2-3, #4-1) or scrambled shRNA (SCR) by quantitative RT-PCR of triplicate RNA samples (bar graph) and western analysis of protein (gels); bands were quantified densitometrically. VEGFR1 RNA and protein levels were normalized on the basis of L32 ribosomal protein mRNA and actin levels, respectively, and expressed relative to controls, which were set at 1.0. (**B**) VEGFR1 knockdown inhibits 344SQ proliferation. Transfectants were seeded in monolayer cultures, counted, and expressed as mean values (± S.D.) of quadruplicate samples. (**C**) VEGFR1 knockdown inhibits CAF-induced tumor cell invasion. Transfectants were co-cultured with CAF; invasive tumor cells were photographed (images) and counted in 5 separate microscopic fields per well, averaged, and mean values per well (± S.D.) were calculated from replicate wells (bar graphs). (**D**) VEGFR1 knockdown inhibits 344SQ anchorage-independent growth. Transfectants were seeded in soft agar, and visible colonies were photographed (images) and counted (bar graph) at 21 days. Results expressed as mean values (± S.D.) of triplicate samples. (**E**) VEGFR1 knockdown inhibits tumor metastasis. Syngeneic mice were injected subcutaneously with tumor cells and necropsied at 6 weeks to measure primary tumor size and count lung metastases (scatter plots). Mean values are represented by long horizontal lines; standard deviations are represented by short horizontal lines. Adapted and reprinted by permission from the American Association for Cancer Research: J.D. Roybal, Y. Zang, and Y.-H, et al., miR-200 Inhibits Lung Adenocarcinoma Cell Invasion and Metastasis by Targeting *Flt1/VEGFR1*, *Mol Cancer Res*, 2010, (9);25, 25-35.
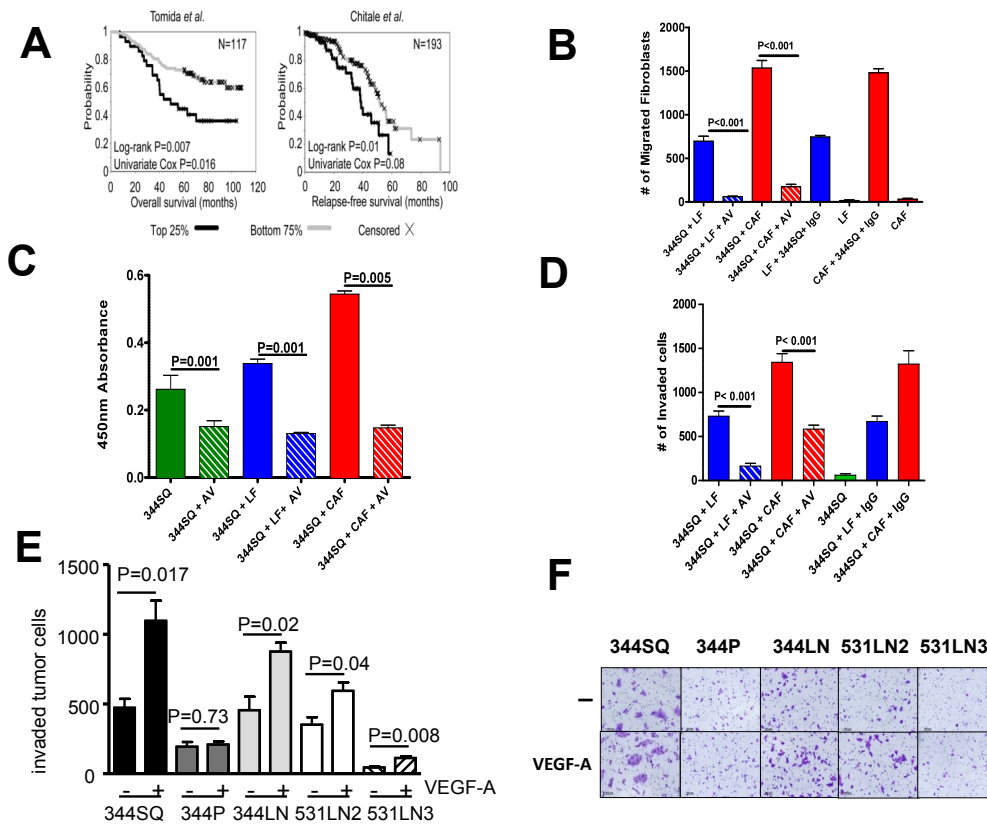
Figure 12. Correlation of VEGFR1 expression with duration of survival and schematic illustration of findings from this study.

(**A**) High VEGR1 expression correlates with a decrease in overall survival and free-relapse survival. Kaplan-Meier analysis of two cohorts of lung adenocarcinoma patients on the basis of VEGFR1 expression (top quartile *versus* lower three quartiles) in resected primary tumor specimens. (**B**) Avastin treatment suppressed migration in co-cultures. Fibroblasts (LF or CAF) were mono-cultured (-) or co-cultured with 344SQ cells and 5 μg/mL of Avastin or IgG. Migrated fibroblasts were counted in at least 5 separate microscopic fields per well, which were averaged, and the mean values per well (± SD) were calculated from replicate wells (bar graphs). Images illustrate representative fields. (**C**) Avastin treatment decreases proliferative rates in mono- and co-cultures. 344SQ cells were seeded at a density of 3.0 X10^4 (n=6 wells per plate); mono- or co-culture conditioned medium plus 5 μg/mL of Avastin or IgG was added to the wells. The proliferative rate was measured with WST-1 reagent after 72 hours. (**D**) Avastin neutralized tumor cell invasion in mono- and co-cultures. 344SQ cells were mono-cultured (-) or co-cultured with LF (LF) or CAF and 5 μg/mL of Avastin or IgG. Invasive tumor cells were photographed (images) and counted in at least 5 separate microscopic fields per well, which were averaged, and the mean values per well (± SD) were calculated from replicate wells (bar graphs). (**E and F**) Tumor cell invasion induced by recombinant VEGF-A. The indicated tumor cell lines derived from Kras$^{LA1/+}$; p53$^{R172H\Delta G/+}$ mice were mono-cultured in the upper chamber of a dual-chamber well, and recombinant VEGF-A was added (+) or not added (-) to the lower chamber. Invasive tumor cells were photographed (images) and quantified(bar graphs) the same way as (**B**). Adapted and reprinted by permission from the American Association for Cancer Research: J.D. Roybal, Y. Zang, and Y.-H, et al., miR-200 Inhibits Lung Adenocarcinoma Cell Invasion and Metastasis by Targeting *Flt1/VEGFR1*, *Mol Cancer Res*, 2010, (9);25, 25-35.

VEGFR1 expression and relapse-free survival in a second cohort (n=193, P=0.01, Log-rank test; P=0.08, univariate Cox, Figure 12A), indicating that VEGFR1 expression may adversely impact the clinical outcome for certain lung adenocarcinoma patient cohorts (Chitale et al., 2009). To further demonstrate that neutralization of VEGFR1 on tumor cells could be beneficial as a lung cancer treatment, we treated *in vitro* co-cultures with 5μg/mL Bevacizumab, also known as Avastin. Bevacizumab is a humanized monoclonal antibody commonly used in the clinic to reduce tumorigenesis in lung adenocarcinoma patients; the antibody binds onto VEGF-A to neutralize the protein and prevent VEGF-A from binding onto its receptor in order to reduce angiogenesis (Yancopoulos, 2010). We used the monoclonal antibody in the co-culture assay and saw a decrease in the migration of CAF and LF toward 344SQ (Figure 12B) and a reduction in 344SQ cell proliferation in monolayer cultures (Figure 12C). Corresponding to the migration assays, we performed *in vitro* invasion assays with 344SQ cells and CAF or LF with the summation of Bevacizumab treatment, which demonstrated a reduction in the invasiveness of 344SQ in response to the presence of CAF or LF (Figure 12D). Given the high levels of VEGF-A relative to that of VEGF-D (712.9 versus 11.7 pg/ml, Table 1), we added recombinant VEGF-A as a chemoattractant to the lower chamber of *in vitro* invasion assays, which enhanced the invasion of four of the five lung adenocarcinoma cell lines examined (Figure 12E). In contrast to our data, which showed that the recombinant peptide is capable of acting as a chemoattractant, applying a VEGF-A neutralizing antibody in *in vitro* co-culture

assays demonstrated a decrease in the migratory potential of fibroblasts toward

tumor cells (Figure 13A) and a decrease of invasiveness of the tumor cells

toward CAF or LF (Figure 13B and 13C). All these findings indicate that the

stimulation of VEGFR1 by VEGF-A is a key signaling pathway within our murine

model of metastatic lung cancer.

VEGFR1 is a miR-200 target gene.

Given our results and previous reports that miR-200 is a master regulator

of EMT and metastasis within this model, we posited that VEGFR1 is a miR-200

target gene (Gibbons et al., 2009b). We tested this hypothesis by co-culturing

CAF with 344SQ cells that were stably transfected with lentiviral vectors

expressing miR-200b/a/429 (344SQ_200b) or nothing (344SQ_vec). Forced

expression of miR-200b in 344SQ cells decreased CAF-induced tumor cell

invasion by 66% (*P*=0.001, two-sided Student's t-test, Figure 14A) and

decreased VEGFR1 mRNA and protein levels by 73% and 38%, respectively,

whereas the mRNA levels of other cytokine receptors did not change Figure

14B). To further validate this hypothesis and the above findings, we examined

whether or not miR-200 decreased VEGFR1 levels by targeting sequences in

the *Flt1* 3'-untranslated region (*3'*-UTR). Analysis using the target scan tool

(www.targetscan.org) revealed two putative miR-200b/c/429 binding sites in the

Flt1 3'-UTR (diagrammatically illustrated in Figure 14C). One is located from

nucleotides 33 to 39 and has similar scores for the *bona fide* miR-200b/c/429

binding sites within the *Zeb1* 3'-UTR with the probability of conserved targeting
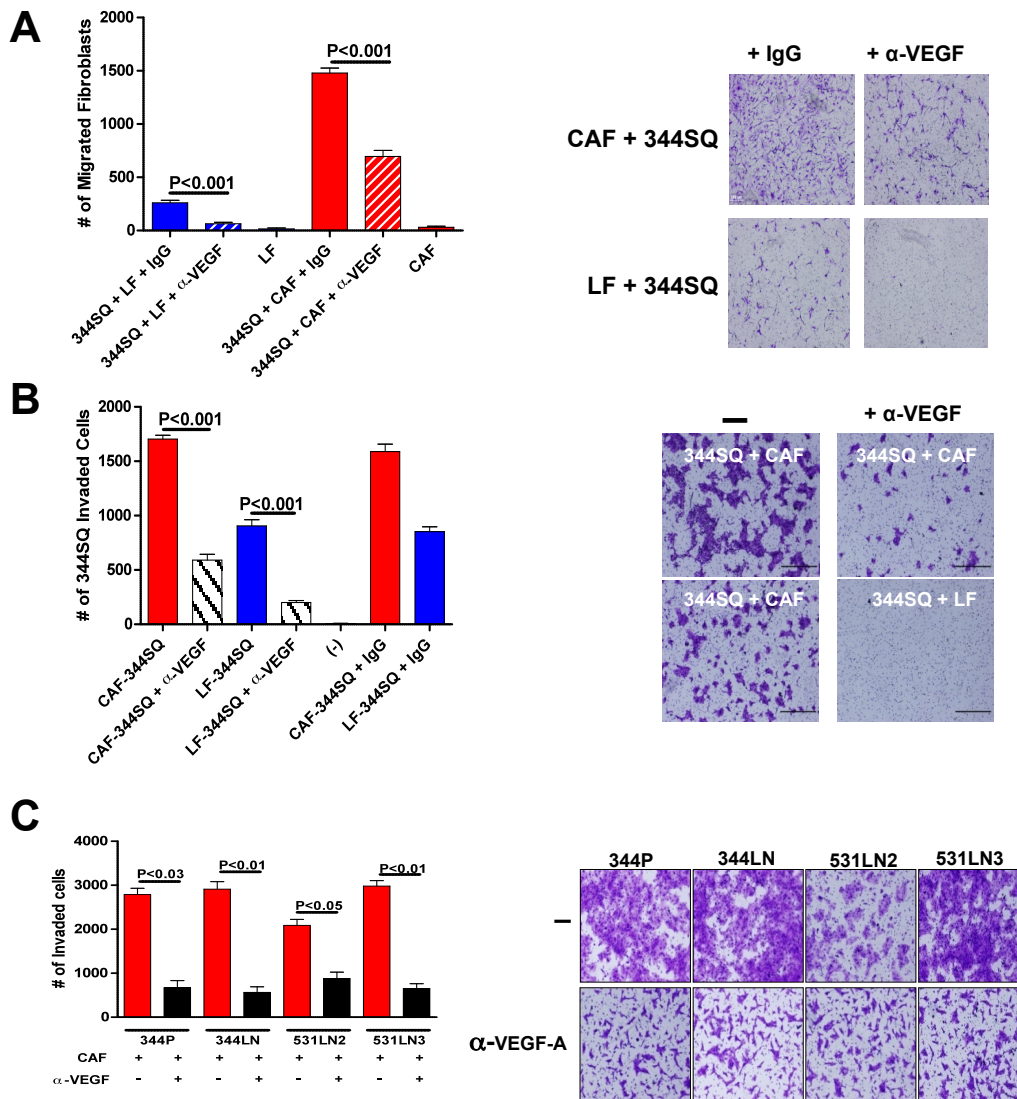
Figure 13: Anti-VEGFR1 reduces tumor cell invasion.
(A) Tumor cell-induced fibroblast migration was reduced by anti-VEGF-A treatment. Anti-VEGF-A or IgG was added (+) or not added (-) to the lower chamber containing 344SQ cells of co-cultures. LF or CAF were photographed (images) and counted in at least 5 separate microscopic fields per well, which were averaged, and the mean values per well (± SD) were calculated from replicate wells (bar graphs). **(B and C)** Tumor cell invasion induced by recombinant VEGF-A. The indicated tumor cell lines derived from Kras[LA1/+]; p53[R172HΔG/+] mice were mono-cultured in the upper chamber of a dual-chamber well, and anti-VEGF-A or IgG was added (+) or not added (-) to the lower chamber. Invasive tumor cells were photographed (images) and counted in at least 5 separate microscopic fields per well, which were averaged, and the mean values per well (± SD) were calculated from replicate wells (bar graphs). Adapted and reprinted by permission from the American Association for Cancer Research: J.D. Roybal, Y. Zang, and Y.-H, et al., miR-200 Inhibits Lung Adenocarcinoma Cell Invasion and Metastasis by Targeting *Flt1/VEGFR1*, *Mol Cancer Res*, 2010, (9);25, 25-35.
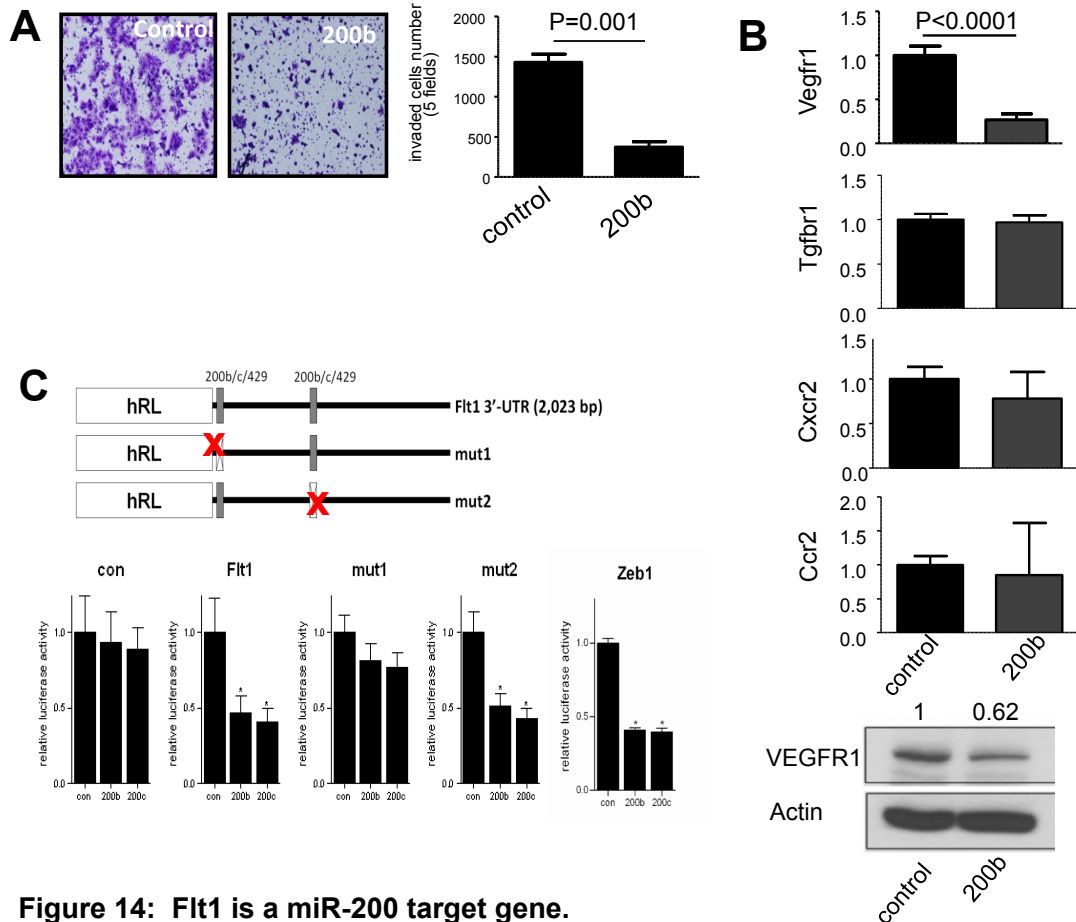
Figure 14: Flt1 is a miR-200 target gene.
(**A**) miR-200 suppresses CAF-induced tumor cell invasion. Transwell invasion assays of 344SQ cells that stably express miR-200b (200b) or empty (control) lentiviral vectors in co-culture with CAF. Invaded cells were stained, photographed (image), and counted in at least 5 separate microscopic fields per well, which were averaged, and the mean values per well (± S.D.) were calculated from replicate wells (bar graph). (**B**) miR-200 suppresses VEGFR1 expression. Quantitative RT-PCR analysis (bar graphs) of 344SQ cells stably transfected with miR-200 (200b) or empty (control) lentiviral vectors normalized on the basis of L32 ribosomal protein mRNA levels and expressed as mean values of triplicate cultures relative to control transfectants, which were set at 1.0. Western blotting (gels) of the same transfectants. Actin included as loading control. VEGFR1 bands were quantified densitometrically, normalized on the basis of actin, and expressed relative to control, set at 1.0. (**C**) miR-200 targets sequences in the *Flt-1* gene *3'*-UTR. Reporter constructs containing wild-type and mutant *Flt1* 3'UTR are illustrated diagrammatically (top). 344SQ cells were transiently co-transfected with pre-miRs (10 nM) and reporter plasmids (500 ng) that express luciferase alone (con) or are linked to the full-length *3'*-UTR of *Zeb1* (*Zeb1*) or *Flt1* that is wild-type (*Flt1*) or mutated at the 5' (mut1) or 3' (mut2) putative miR-200 binding site. Results were normalized on the basis of renilla luciferase and expressed as the mean values of triplicate wells (* $p < 0.05$). Adapted and reprinted by permission from the American Association for Cancer Research: J.D. Roybal, Y. Zang, and Y.-H, et al., miR-200 Inhibits Lung Adenocarcinoma Cell Invasion and Metastasis by Targeting *Flt1/VEGFR1*, *Mol Cancer Res*, 2010, (9);25, 25-35.

score or P_{CT} score (Friedman et al., 2009) of 0.84, and the other is located from nucleotides 847 to 853 and has a P_{CT} score < 0.10. In contrast, no putative miR-200 binding sites with P_{CT} scores > 0.80 were found within the 3'-UTR of genes encoding CCR1, CCR2, CCR5, CXCR2, CXCR3, type I and II TGFβ receptors, IL6Rα, IL18R1, or c-Fms.   In addition to testing a negative control in 344SQ cells, we created a positive reporter plasmid containing a luciferase fused to *3'*-UTR sequences from *Flt1* and *Zeb1* and generated our hypothesis-testing cells by transiently co-transfecting 344SQ cells with synthetic miR-200 precursors (200a, 200b, 200c, 141, or 429)(Figure 14C). After comparing miR-200b and miR-200c to scrambled control oligomers (negative control luciferase reporter), we observed a decrease of 50-60% in the luciferase activity of the *FLT1 3'*-UTR, which was similar to the *Zeb1 3'*-UTR reporter (positive control)(Figure 14C). The site-directed mutagenesis of the 5' putative miR-200 binding site negated this suppression of luciferase activity, but the 3' binding site had no effect (Figure 14C). We demonstrated that the regulation of VEGFR1 is specific to miR-200b and miR-200c, because miR-200a and miR-429 (other miR-200 family members) did not have an effect on the *FLT1 3'*-UTR luciferase reporter activity (Data not shown).

Chapter Four

Discussion

Comparative studies on CAF and normal tissue counterparts from a variety of epithelial organs have revealed striking functional and phenotypic differences, including opposing roles in tumorigenesis (Begley et al., 2008; Bhowmick et al., 2004a; Bhowmick et al., 2004b; Trimboli et al., 2009). These data indicate that tumors contain heterogeneous fibroblast populations with diverse and even conflicting effects on tumor cells. We explored the quantitative, phenotypic, and functional differences between normal and cancer-associated lung fibroblasts in mouse models of lung adenocarcinoma and found differences with respect to abundance, myofibroblast features, rates of proliferation, diversity and abundance of secreted proteins, and interactions with tumor cells. Although when comparing the individual cells within the population of cells, the CAF and LF populations appear to be homogeneous on the basis of morphology and marker expression, these findings do not exclude the possibility of biologically or phenotypically distinct fibroblast subpopulations within the larger Thy1[Pos] fibroblast pool. The phenotypic and functional diversity of normal lung fibroblasts, which have been subdivided on the basis of their expression of Thy1, cyclooxygenase-2, and telomerase, supports this possibility (Hardie et al., 2009). Although this presents a complicated picture with respect to the potential role of lung fibroblasts in the development of lung malignancy, our findings clearly demonstrate that a Thy1[Pos]-specific CAF population promotes tumor growth and invasion. These cells share phenotypic and functional features with a Thy1[Pos] CAF population reported in human lung cancers (Nazareth et al., 2007). Although their origin is uncertain, the CAF

reported here may arise from lung fibroblasts or other Thy1[Pos] cells originating from the bone marrow, such as CD45[Pos] Col1[Pos] CXCR4[Pos] fibrocytes that traffic to wounded areas of the lung in response to injury (Craig et al., 1993; Phillips et al., 2004).

A growing body of evidence demonstrates that CAF recruit macrophages and endothelial cells and thereby regulate tumor inflammation and angiogenesis (Erez et al.; Nazareth et al., 2007). Similarly, findings from conditioned medium samples revealed that CAF secrete a plethora of cytokines, chemokines, and growth factors that can recruit endothelial cells (VEGF-A, KC, and MIP-2) or regulate inflammatory cell recruitment and function (MCP-1, MIP1α, MIP-1β, KC, MIP-2, M-CSF, TGFβ1, and interleukin-6). Furthermore, we examined direct interactions between tumor cells and CAF by establishing *in vitro* co-culture models and *in vivo* co-injection models and found that CAF potently induced tumor cell invasion and enhanced tumor growth in mice. Cytokines secreted by CAF that could have mediated these effects include TGFβ1, which induces tumor cells from these mice to undergo EMT (Gibbons et al., 2009b), and VEGF-A, which was sufficient to chemoattract tumor cells in invasion assays and was required for CAF-induced tumor cell invasion (Figure 15). Findings from VEGFR1 knockdown experiments support the conclusion that VEGF-A promotes tumor cell proliferation and invasion *in vitro* and tumor growth and metastasis in mice. Collectively, these findings demonstrate that CAF secrete multiple cytokines that induce tumor cells to undergo diverse biologic processes that promote tumorigenesis, illustrated

51

Summary of Findings
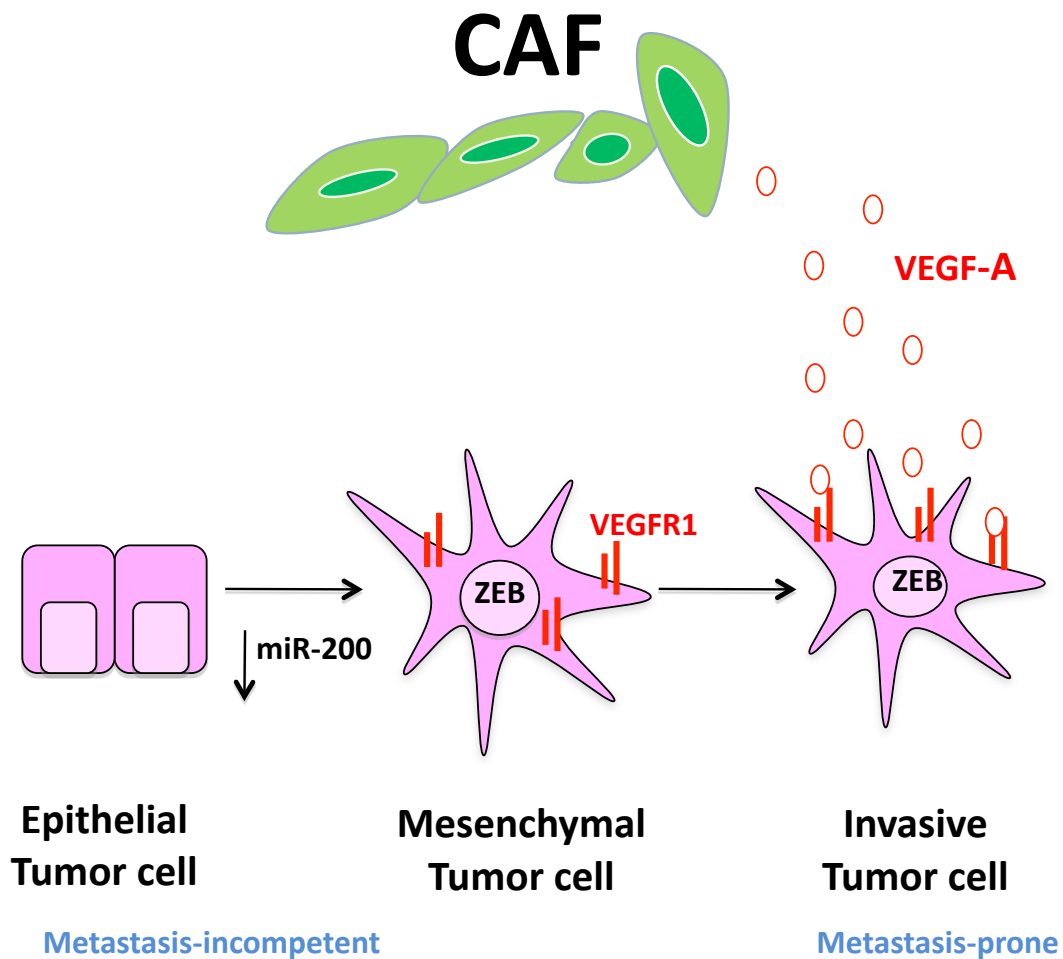
Figure 15: Model that summarizes our findings.
Schematic illustration shows CAF-derived cytokines binding directly to receptors on tumor cells and inducing tumor cells to suppress miR-200 levels, to undergo EMT (TGF-beta), and to invade (VEGF-A).

schematically in Figure 15. After identifying functional interactions between

tumor cells and CAF that drive tumor progression, we tested the hypothesis that

miR-200 targets receptors on tumor cells that transmit paracrine signals from

CAF. The findings presented here support the conclusion that miR-200

regulates tumor cell sensitivity to VEGF-A by directly targeting VEGFR1 (Figure

15). Given that miR-200 had heretofore been recognized solely for its capacity

to regulate EMT in a cell-autonomous manner, our results demonstrate a multi-

functional role for miR-200 and further support a current paradigm that suggests

that tumor cells acquire multiple biologic properties by targeting a single miR

(Gregory et al., 2008; Park et al., 2008). The *bona fide* miR-200 target genes

reported thus far include ZEB1 and ZEB2, which transcriptionally regulate EMT

markers, tight junctional elements, various polarity genes, and *USH/FOG2*, an

inhibitor of the p85 regulatory subunit of phosphotidylinositol 3-kinase (Gibbons

et al., 2009b; Bracken et al., 2008; Burk et al., 2008; Hyun et al., 2009). The

complexity of the miR-200 transcriptome in this model, which encompasses

over 3,000 genes that encode proteins with diverse intracellular functions,

warrants further studies to discover other miR-200 target genes that regulate

tumorigenesis (Gibbons et al., 2009b). The finding that VEGFR1 was not

sufficient to restore metastasis in tumor cells that constitutively express miR-

200 supports the multiplicity of those miR-200 target genes. On a speculative

note, undiscovered miR-200 target genes might include chemokines and

cytokines secreted by tumor cells that chemoattract CAF and other cell types to

the microenvironment would create a negative feedback loop in which miR-200

interrupts the cell-cell interactions that induce tumor cells to undergo EMT and metastasize.

VEGF-A neutralizing antibodies have been proven efficacious as single agents in patients with renal cell carcinomas because they inactivate *VHL* gene mutations that constitutively activate hypoxia-inducible factorα and drive VEGF expression; these antibodies have also been effective in combination with chemotherapeutic agents in patients with *VHL*-wild-type tumors, such as non-small cell lung cancer and colon cancer (Bose et al., 2010). The therapeutic efficacy of VEGF antagonists has been attributed primarily to a suppression of tumor angiogenesis by reducing the chemoattraction of endothelial cells, pericytes, and hematopoietic precursors that express VEGFR1. A growing body of evidence in other models demonstrates that VEGF-A directly promotes tumor cell invasion, and our findings suggest that these agents may have the additional therapeutic benefit of decreasing tumor cell sensitivity to VEGF-A (Wey et al., 2005; Lichtenberger et al.; Naik et al., 2009).

Chapter Five

Future Directions

The cell of origin.

Our findings clearly indicate that Thy1^{Pos} fibroblasts are important cells within the tumor microenvironment because they can signal the tumor cell through cytokine, chemokine, and growth factor networks to aid in processes that govern metastases. CAF have multiple cells-of-origin, including resident fibroblasts, endothelial cells, adipocytes, and bone marrow-derived mesenchymal cells (Wu and Zhou, 2009; Wipff et al., 2007; Hinz, 2007; Hinz et al., 2007).   To our knowledge the origin of the Thy1^{Pos} lung fibroblast has not been fully elucidated in normal and cancerous lungs of mice. Many cell types express Thy1 as a cell-surface marker, and because leukocytes and T-cells express Thy1, we hypothesized that resident Thy1^{Pos} lung fibroblasts were derived from the bone marrow. We addressed this question by lethally irradiating wildtype 129/SV mice to remove their native bone marrow; after grafting the mice with constitutive YFP bone marrow (BM-YFP^{Pos}) from B6.Cg-Tg(EYFP)AGfng/J mice, at greater than 80% engraftment (Figure 17A), we orthotopically injected these mice with 2.0 X10^4 344SQ cells for three weeks (shown in Figure 16). 344SQ cells were used as a chemoattractant to draw the BM-YFP^{Pos} cells to the lungs. We performed FACS analysis to isolate and analyze the cells using a gating strategy that separated first the hematopoietic cells from large granular cells and then subgated those cells that were double positive for Thy1 and YFP and CD45^{Neg}. The results showed that a greater proportion of these Thy1^{Pos}YFP^{Pos}CD45^{Neg} cells were mostly small in

Bone Marrow Experimental Design
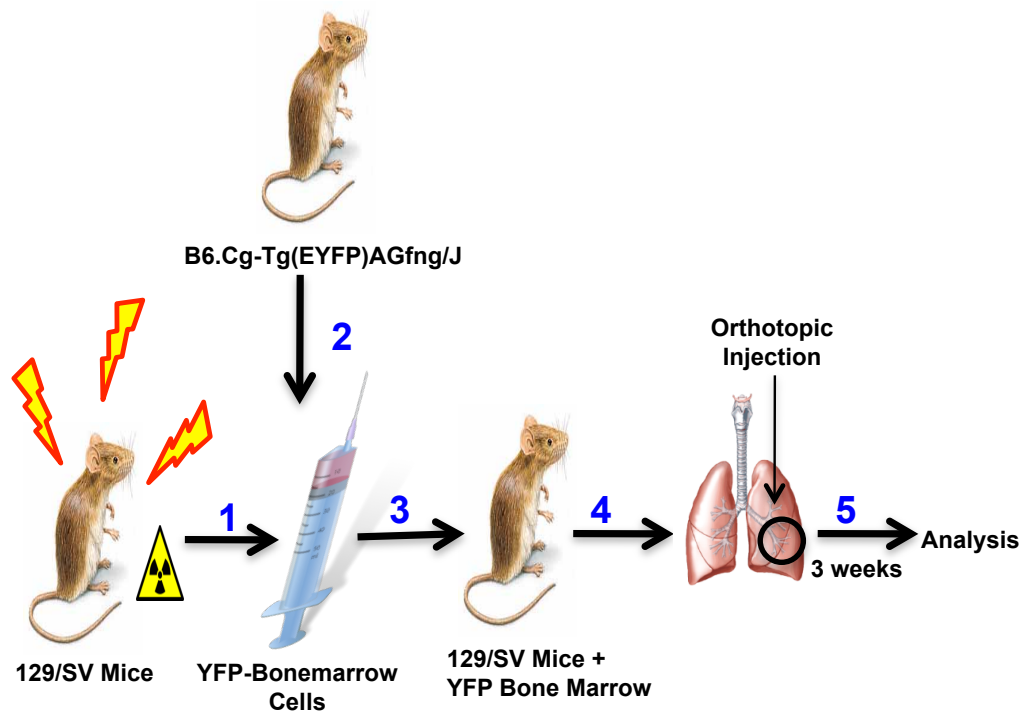
Figure 16: Bone Marrow-derived fibroblast experimental design.
(1-3)129/SV mice were lethally irradiated and engrafted with bone marrow from B6.Cg-Tg (EYFP)AGfng/J mice that express constitutive expression of YFP. **(4)** The mice that had greater than 80% reconstitution of the YFP bone marrow were subjected to orthotopic injection of 344SQ cells (2.0×10^4 cells) or none at all. **(5)** The mice were sacrificed three weeks post-surgical operation. Total mice were n=10 for injected and n=10 for non-injected mice.
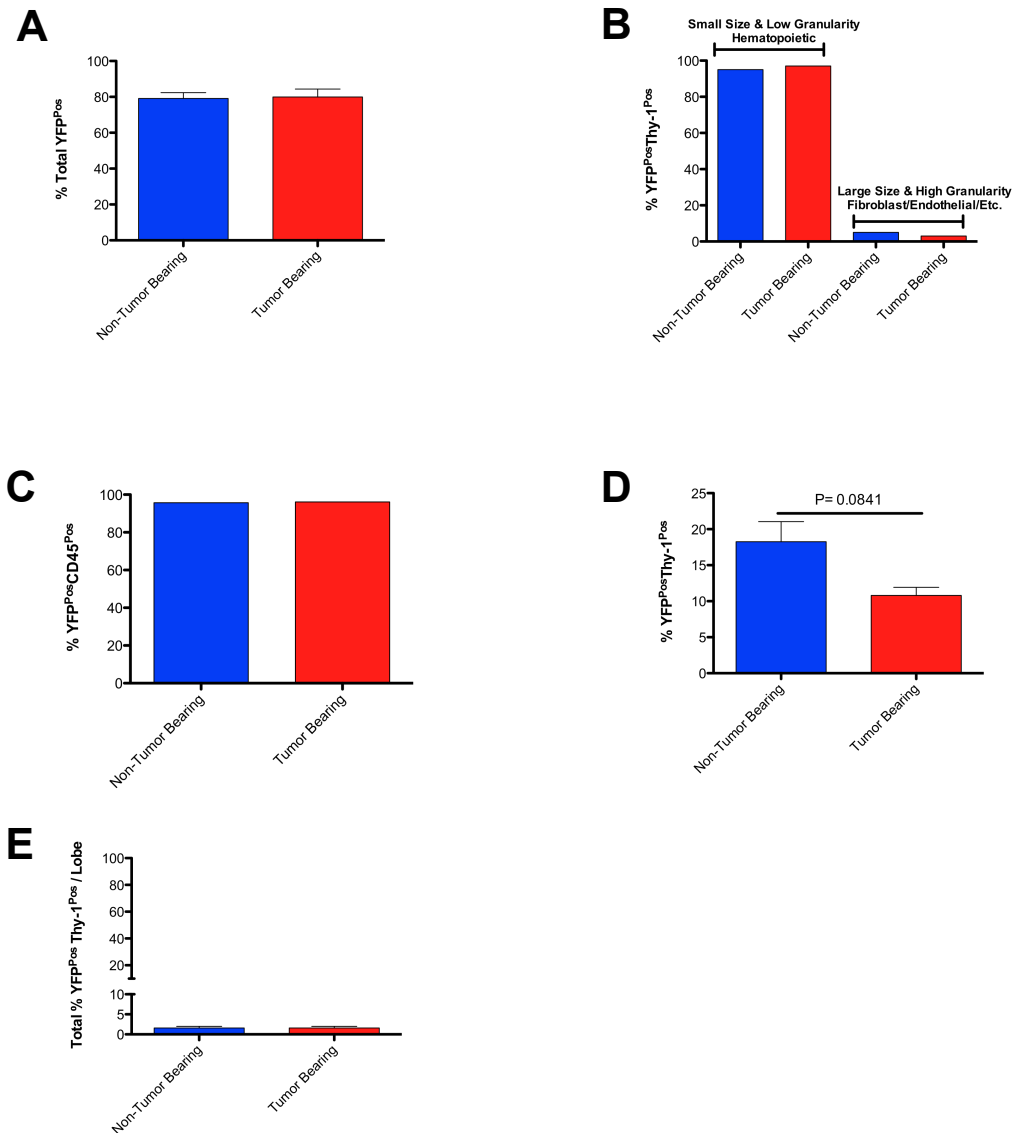
Figure 17: Bone-Marrow Derived CAF studies.
(A) Lethally irradiated with YFP engrafted bone marrow cells demonstrated greater than or equal to eighty percent reconstitution. Peripheral blood was taken from the tails of reconstituted mice and subject to flow cytometry analysis for YFP positive cells. Results are shown with the results of six mice. **(B and C)** The bulk of the cells, greater than ninety-one percent of YFP+ cells, are hematopoietic as demonstrated by the broad hematopoietic marker CD45. Mice were sacrificed 3 weeks post orthotopic injection or non-injection of 344SQ cells into the lungs. Cells enzymatically digested into a single-cell suspension and subjected to FACs analysis for YFP^{Pos}Thy1^{Pos}CD45^{Neg} cells. **(D)** There are more YFP^{Pos}Thy1^{Pos} cells in non-injected mice than in injected mice. Quantification were expressed as a percent between the two groups. **(E)** YFP^{Pos}Thy1^{Pos}CD45^{Neg} cells are a rare population in these mice. Totals were expressed as percentages from total quantification.

size (Figure 17) and likely to be hematopoietic cells (Figures 17B and 17C).

Moreover, there was an increase in double positive Thy1^{Pos}- YFP^{Pos} cells in the

non-injected mice when compared to those mice that had been orthotopically

injected (Figure 17D). The data demonstrate that these cells are a rare

population in these mice, in comparison to the overall percentage of cells in the

lungs (Figure 17E). Unfortunately, all the cells in the bone marrow of these mice

constitutively express YFP, and YFP is not driven by a promoter that is specific

for Thy1 or for bone marrow cells; this allows for background when collecting

the cells and analyzing the data from those results. A more elegant experiment

would use the bone marrow from mice that express YFP under the control of

the Thy1 promoter, which would definitely identify whether the tumor cells were

able to chemoattract the Thy1^{Pos} bone marrow cells. Additionally, colocalization

studies with YFP and different colored markers for fibroblasts, such as FSP-1

and α-SMA, would definitively identify whether or not the fibroblast cells were

bone marrow-derived. However, taken together these data suggest that only a

very small percentage of the Thy1^{Pos} fibroblasts could be BM-derived (Figure

17E), which leads us to speculate further that these cells could be precursor

fibroblasts that are changed into CAF in the tumor microenvironment.

Others have also shown that CAF are derived from precursor fibroblasts

that are resident in the normal tissue and become CAF upon tumorigenesis

formation(Wu and Zhou, 2009; Wipff et al., 2007; Hinz, 2007; Hinz et al., 2007;

Grivennikov et al., 2010). More specifically, recent studies have demonstrated

that certain secreted soluble factors are capable of re-educating fibroblasts to a

CAF phenotype by taking conditioned media from cancer cells and placing it on normal fibroblasts to elicit the change to a CAF (Erez et al., 2010). The current published data and our recent findings in the bone marrow experiments lead us to speculate that LF have been re-educated within the tumor microenvironment to become CAF. As previously demonstrated by other groups, a series of similar experiments could be performed to identify whether or not this is the case by adding CAF conditioned medium or 344SQ conditioned medium to LF cultures and using our *in vitro* migration and invasion experiments as a readout. Additionally, immunofluorescence staining for increased expression of α-SMA and Vimentin expression would identify whether or not these cells become activated to a myofibroblast state. Taken together, all these data would further validate the hypothesis that the soluble secreted factors within a particular microenvironment could elicit a fibroblast to become a pro-cancerous fibroblast.

Three-dimensional cultures.

Current research has focused on the type of assays that comprise the microenvironment in which we culture our cells and run our assays. It is becoming more recognized that the cells respond differently in three-dimensional assay compared to a two-dimensional type system (Gibbons et al., 2009b; Grimshaw et al., 2008). To test this aspect we used a previously published three-dimensional assay, an *in vitro* sphere assay in which 344SQ cells are placed on growth factor reduced Matrigel in normal culturing conditions (Gibbons et al., 2009b). When the cells are in those conditions, 344SQ express

typical polarity markers and form a hollow sphere with distinct morphology and grow to about 100μm in size (Gibbons et al., 2009b). To identify whether or not LF or CAF had a morphological effect on 344SQ cells in three-dimensional cultures, we co-cultured 344SQ cells with LF ad CAF in the sphere assay (Gibbons et al., 2009b). Co-culturing CAF with 344SQ spheres demonstrated a change in the spheres' morphology from round hollow spheres to non-round spheres with irregular elongated projections (Figure 18A); when LF was co-cultured with 344SQ, the spheres' morphology did not change (Figure 18A). These results from the three-dimensional assays suggest that these CAF are contributing to the pro-cancerous phenotype either through direct cell-cell contacts or by some other mechanism, such as their extracellular matrix environment.

CAF secrete a pro-cancerous extracellular matrix.

The soluble secreted factors are important not only within the tumor microenvironment but also in the native niche that encompasses the tumor, such as the extracellular matrix. It is well-known and accepted that fibroblasts secrete extracellular matrix molecules (collagen, elastin, and fibronectin, etc) that provide the structural integrity of the basal lamina in the normal pathology of the tissues. On that note it has also been documented that CAF can secrete extracellular matrices that are pro-tumorigenic in breast cancer models

A

B

344SQ-GFP

+ CAF ECM   + CAF ECM   —
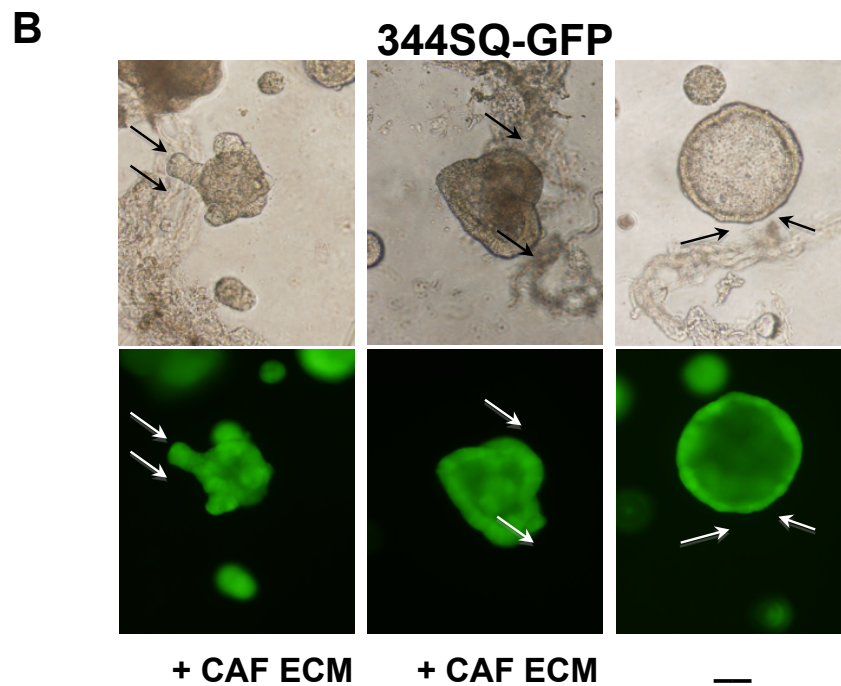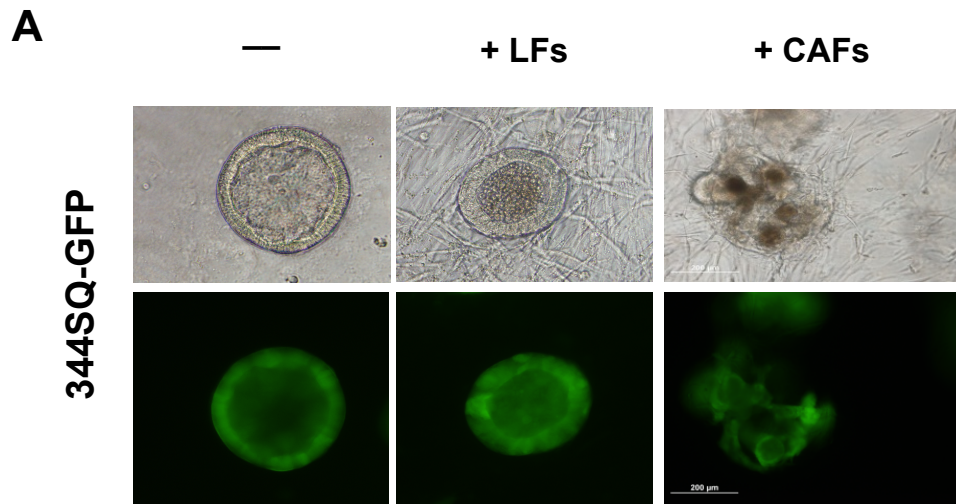
Figure 18: CAF and CAF-derived matrix causes morphological changes in 344SQ spheres.
A) Fibroblast-induced tumor sphere morphology changes. GFP-tagged 344SQ spheres in mono-culture (-) or co-culture with fibroblasts (LF, CAF). Coordinate fields visualized by light (top) or immunofluorescence (bottom) confocal microscopy (40x). Bar indicates 200 μm. **(B)** CAF matrix-induced tumor sphere morphology changes. GFP-tagged 344SQ spheres in mono-culture (-) or co-culture with matrix derived from CAF. Coordinate fields visualized by light (top) or immunofluorescence (bottom) confocal microscopy (40x). Bar indicates 200 μm.

(Castello-Cros et al., 2009). A previously published method allowed us to

isolate the extracellular matrix from both LF and CAF (Castello-Cros and

Cukierman, 2009). When we placed the CAF matrix on top of 344SQ spheres in

the sphere assay, the matrix induced a morphological change in the spheres

(Figure 18B). Because the matrix had to be in direct contact with the sphere in

order to cause a morphological change (clearly demonstrated in Figure 18B),

we speculate that the extracellular matrix laid down by CAF is also critically

important to the cancerous phenotype. Future studies are needed to identify the

differences between the LF and CAF matrices to identify the potential

molecules that can regulate the morphological change within these three-

dimensional assays. These findings elicit an exciting new branch of studies

within the metastatic tumor microenvironment.

References:

1.   Jemal, A., Center, M. M., DeSantis, C., and Ward, E. M. (2010a). Global patterns of cancer incidence and mortality rates and trends. Cancer Epidemiol Biomarkers Prev *19*, 1893-1907.

2.   Jemal, A., Siegel, R., Xu, J., and Ward, E. (2010b). Cancer statistics, 2010. CA Cancer J Clin *60*, 277-300.

3.   Gibbons, D. L., Lin, W., Creighton, C. J., Zheng, S., Berel, D., Yang, Y., Raso, M. G., Liu, D. D., Wistuba, II, Lozano, G., and Kurie, J. M. (2009a). Expression signatures of metastatic capacity in a genetic mouse model of lung adenocarcinoma. PLoS One *4*, e5401.

4.   Roybal, J. D., Zang, Y., Ahn, Y. H., Yang, Y., Gibbons, D. L., Baird, B. N., Alvarez, C., Thilaganathan, N., Liu, D. D., Saintigny, P., Heymach, J. V., Creighton, C. J., and Kurie, J. M. (2011). miR-200 Inhibits lung adenocarcinoma cell invasion and metastasis by targeting Flt1/VEGFR1. Mol Cancer Res *9*, 25-35.

5.   Mantovani, A., Sica, A., Sozzani, S., Allavena, P., Vecchi, A., and Locati, M. (2004). The chemokine system in diverse forms of macrophage activation and polarization. Trends Immunol *25*, 677-686.

6.   Mantovani, A., Sozzani, S., Locati, M., Allavena, P., and Sica, A. (2002). Macrophage polarization: tumor-associated macrophages as a paradigm for polarized M2 mononuclear phagocytes. Trends Immunol *23*, 549-555.

7.   Shimoda, M., Mellody, K. T., and Orimo, A. (2010). Carcinoma-associated fibroblasts are a rate-limiting determinant for tumour progression. Semin Cell Dev Biol *21*, 19-25.

8.   Wu, Y., and Zhou, B. P. (2009). Inflammation: a driving force speeds cancer metastasis. Cell Cycle *8*, 3267-3273.

9.   Zhou, B. B., Peyton, M., He, B., Liu, C., Girard, L., Caudler, E., Lo, Y., Baribaud, F., Mikami, I., Reguart, N., Yang, G., Li, Y., Yao, W., Vaddi, K., Gazdar, A. F., Friedman, S. M., Jablons, D. M., Newton, R. C., Fridman, J. S., Minna, J. D., and Scherle, P. A. (2006). Targeting ADAM-mediated ligand cleavage to inhibit HER3 and EGFR pathways in non-small cell lung cancer. Cancer Cell *10*, 39-50.

10.   Desmouliere, A., Guyot, C., and Gabbiani, G. (2004). The stroma reaction myofibroblast: a key player in the control of tumor cell behavior. Int J Dev Biol *48*, 509-517.

11.   Sugimoto, H., Mundel, T. M., Kieran, M. W., and Kalluri, R. (2006). Identification of fibroblast heterogeneity in the tumor microenvironment. Cancer Biol Ther *5*, 1640-1646.

12.   Chang, H. Y., Sneddon, J. B., Alizadeh, A. A., Sood, R., West, R. B., Montgomery, K., Chi, J. T., van de Rijn, M., Botstein, D., and Brown, P. O. (2004). Gene expression signature of fibroblast serum response predicts human cancer progression: similarities between tumors and wounds. PLoS Biol *2*, E7.

13.   Santos, A. M., Jung, J., Aziz, N., Kissil, J. L., and Pure, E. (2009).
       Targeting fibroblast activation protein inhibits tumor stromagenesis and
       growth in mice. J Clin Invest *119*, 3613-3625.

14.   Erez, N., Truitt, M., Olson, P., Arron, S. T., and Hanahan, D. (2010).
       Cancer-Associated Fibroblasts Are Activated in Incipient Neoplasia to
       Orchestrate Tumor-Promoting Inflammation in an NF-kappaB-Dependent
       Manner. Cancer Cell *17*, 135-147.

15.   Nazareth, M. R., Broderick, L., Simpson-Abelson, M. R., Kelleher, R. J.,
       Jr., Yokota, S. J., and Bankert, R. B. (2007). Characterization of human
       lung tumor-associated fibroblasts and their ability to modulate the
       activation of tumor-associated T cells. J Immunol *178*, 5552-5562.

16.   Anderberg, C., Li, H., Fredriksson, L., Andrae, J., Betsholtz, C., Li, X.,
       Eriksson, U., and Pietras, K. (2009). Paracrine signaling by platelet-
       derived growth factor-CC promotes tumor growth by recruitment of
       cancer-associated fibroblasts. Cancer Res *69*, 369-378.

17.   Gibbons, D. L., Lin, W., Creighton, C. J., Rizvi, Z. H., Gregory, P. A.,
       Goodall, G. J., Thilaganathan, N., Du, L., Zhang, Y., Pertsemlidis, A.,
       and Kurie, J. M. (2009b). Contextual extracellular cues promote tumor
       cell EMT and metastasis by regulating miR-200 family expression.
       Genes Dev *23*, 2140-2151.

18.   Shenouda, S. K., and Alahari, S. K. (2009). MicroRNA function in cancer:
       oncogene or a tumor suppressor? Cancer Metastasis Rev *28*, 369-378.

19.   Carletti, M. Z., and Christenson, L. K. (2009). MicroRNA in the ovary and female reproductive tract. J Anim Sci *87*, E29-38.

20.   Wipff, P. J., Rifkin, D. B., Meister, J. J., and Hinz, B. (2007). Myofibroblast contraction activates latent TGF-beta1 from the extracellular matrix. J Cell Biol *179*, 1311-1323.

21.   Rege, T. A., and Hagood, J. S. (2006). Thy-1, a versatile modulator of signaling affecting cellular adhesion, proliferation, survival, and cytokine/growth factor responses. Biochim Biophys Acta *1763*, 991-999.

22.   Hardie, W. D., Glasser, S. W., and Hagood, J. S. (2009). Emerging concepts in the pathogenesis of lung fibrosis. Am J Pathol *175*, 3-16.

23.   Wislez, M., Fujimoto, N., Izzo, J. G., Hanna, A. E., Cody, D. D., Langley, R. R., Tang, H., Burdick, M. D., Sato, M., Minna, J. D., Mao, L., Wistuba, I., Strieter, R. M., and Kurie, J. M. (2006). High expression of ligands for chemokine receptor CXCR2 in alveolar epithelial neoplasia induced by oncogenic kras. Cancer Res *66*, 4198-4207.

24.   Yoshikura, H., and Hirokawa, Y. (1974). Endogenous C-type virus of a mouse cell line and its defectiveness. J Virol *13*, 1319-1325.

25.   Zhong, L., Roybal, J., Chaerkady, R., Zhang, W., Choi, K., Alvarez, C. A., Tran, H., Creighton, C. J., Yan, S., Strieter, R. M., Pandey, A., and Kurie, J. M. (2008). Identification of secreted proteins that mediate cell-cell interactions in an in vitro model of the lung cancer microenvironment. Cancer Res *68*, 7237-7245.

26.   McQualter, J. L., Brouard, N., Williams, B., Baird, B. N., Sims-Lucas, S., Yuen, K., Nilsson, S. K., Simmons, P. J., and Bertoncello, I. (2009). Endogenous fibroblastic progenitor cells in the adult mouse lung are highly enriched in the sca-1 positive cell fraction. Stem Cells *27*, 623-633.

27.   Porter, D., Lahti-Domenici, J., Keshaviah, A., Bae, Y. K., Argani, P., Marks, J., Richardson, A., Cooper, A., Strausberg, R., Riggins, G. J., Schnitt, S., Gabrielson, E., Gelman, R., and Polyak, K. (2003). Molecular markers in ductal carcinoma in situ of the breast. Mol Cancer Res *1*, 362-375.

28.   Castello-Cros, R., and Cukierman, E. (2009). Stromagenesis during tumorigenesis: characterization of tumor-associated fibroblasts and stroma-derived 3D matrices. Methods Mol Biol *522*, 275-305.

29.   Liao, D., Luo, Y., Markowitz, D., Xiang, R., and Reisfeld, R. A. (2009). Cancer associated fibroblasts promote tumor growth and metastasis by modulating the tumor immune microenvironment in a 4T1 murine breast cancer model. PLoS One *4*, e7965.

30.   Zhang, Y., Tang, H., Cai, J., Zhang, T., Guo, J., Feng, D., and Wang, Z. (2011). Ovarian cancer-associated fibroblasts contribute to epithelial ovarian carcinoma metastasis by promoting angiogenesis, lymphangiogenesis and tumor cell invasion. Cancer Lett *303*, 47-55.

31.   Zeine, R., Salwen, H. R., Peddinti, R., Tian, Y., Guerrero, L., Yang, Q., Chlenski, A., and Cohn, S. L. (2009). Presence of cancer-associated

fibroblasts inversely correlates with Schwannian stroma in neuroblastoma tumors. Mod Pathol *22*, 950-958.

32. Johnson, L., Mercer, K., Greenbaum, D., Bronson, R. T., Crowley, D., Tuveson, D. A., and Jacks, T. (2001). Somatic activation of the K-ras oncogene causes early onset lung cancer in mice. Nature *410*, 1111-1116.

33. Mishra, P., Banerjee, D., and Ben-Baruch, A. (2011). Chemokines at the crossroads of tumor-fibroblast interactions that promote malignancy. J Leukoc Biol *89*, 31-39.

34. Chitale, D., Gong, Y., Taylor, B. S., Broderick, S., Brennan, C., Somwar, R., Golas, B., Wang, L., Motoi, N., Szoke, J., Reinersman, J. M., Major, J., Sander, C., Seshan, V. E., Zakowski, M. F., Rusch, V., Pao, W., Gerald, W., and Ladanyi, M. (2009). An integrated genomic analysis of lung cancer reveals loss of DUSP4 in EGFR-mutant tumors. Oncogene *28*, 2773-2783.

35. Tomida, S., Takeuchi, T., Shimada, Y., Arima, C., Matsuo, K., Mitsudomi, T., Yatabe, Y., and Takahashi, T. (2009). Relapse-related molecular signature in lung adenocarcinomas identifies patients with dismal prognosis. J Clin Oncol *27*, 2793-2799.

36. Yancopoulos, G. D. (2010). Clinical application of therapies targeting VEGF. Cell *143*, 13-16.

37.   Friedman, R. C., Farh, K. K., Burge, C. B., and Bartel, D. P. (2009). Most mammalian mRNAs are conserved targets of microRNAs. Genome Res *19*, 92-105.

38.   Begley, L. A., Kasina, S., MacDonald, J., and Macoska, J. A. (2008). The inflammatory microenvironment of the aging prostate facilitates cellular proliferation and hypertrophy. Cytokine *43*, 194-199.

39.   Bhowmick, N. A., Chytil, A., Plieth, D., Gorska, A. E., Dumont, N., Shappell, S., Washington, M. K., Neilson, E. G., and Moses, H. L. (2004a). TGF-beta signaling in fibroblasts modulates the oncogenic potential of adjacent epithelia. Science *303*, 848-851.

40.   Bhowmick, N. A., Neilson, E. G., and Moses, H. L. (2004b). Stromal fibroblasts in cancer initiation and progression. Nature *432*, 332-337.

41.   Trimboli, A. J., Cantemir-Stone, C. Z., Li, F., Wallace, J. A., Merchant, A., Creasap, N., Thompson, J. C., Caserta, E., Wang, H., Chong, J. L., Naidu, S., Wei, G., Sharma, S. M., Stephens, J. A., Fernandez, S. A., Gurcan, M. N., Weinstein, M. B., Barsky, S. H., Yee, L., Rosol, T. J., Stromberg, P. C., Robinson, M. L., Pepin, F., Hallett, M., Park, M., Ostrowski, M. C., and Leone, G. (2009). Pten in stromal fibroblasts suppresses mammary epithelial tumours. Nature *461*, 1084-1091.

42.   Craig, W., Kay, R., Cutler, R. L., and Lansdorp, P. M. (1993). Expression of Thy-1 on human hematopoietic progenitor cells. J Exp Med *177*, 1331-1342.

43. Phillips, R. J., Burdick, M. D., Hong, K., Lutz, M. A., Murray, L. A., Xue, Y. Y., Belperio, J. A., Keane, M. P., and Strieter, R. M. (2004). Circulating fibrocytes traffic to the lungs in response to CXCL12 and mediate fibrosis. J Clin Invest *114*, 438-446.

44. Gregory, P. A., Bert, A. G., Paterson, E. L., Barry, S. C., Tsykin, A., Farshid, G., Vadas, M. A., Khew-Goodall, Y., and Goodall, G. J. (2008). The miR-200 family and miR-205 regulate epithelial to mesenchymal transition by targeting ZEB1 and SIP1. Nat Cell Biol *10*, 593-601.

45. Park, S. M., Gaur, A. B., Lengyel, E., and Peter, M. E. (2008). The miR-200 family determines the epithelial phenotype of cancer cells by targeting the E-cadherin repressors ZEB1 and ZEB2. Genes Dev *22*, 894-907.

46. Bracken, C. P., Gregory, P. A., Kolesnikoff, N., Bert, A. G., Wang, J., Shannon, M. F., and Goodall, G. J. (2008). A double-negative feedback loop between ZEB1-SIP1 and the microRNA-200 family regulates epithelial-mesenchymal transition. Cancer Res *68*, 7846-7854.

47. Burk, U., Schubert, J., Wellner, U., Schmalhofer, O., Vincan, E., Spaderna, S., and Brabletz, T. (2008). A reciprocal repression between ZEB1 and members of the miR-200 family promotes EMT and invasion in cancer cells. EMBO Rep *9*, 582-589.

48. Hyun, S., Lee, J. H., Jin, H., Nam, J., Namkoong, B., Lee, G., Chung, J., and Kim, V. N. (2009). Conserved MicroRNA miR-8/miR-200 and its

target USH/FOG2 control growth by regulating PI3K. Cell *139*, 1096-1108.

49.   Bose, D., Meric-Bernstam, F., Hofstetter, W., Reardon, D. A., Flaherty, K. T., and Ellis, L. M. (2010). Vascular endothelial growth factor targeted therapy in the perioperative setting: implications for patient care. Lancet Oncol *11*, 373-382.

50.   Wey, J. S., Fan, F., Gray, M. J., Bauer, T. W., McCarty, M. F., Somcio, R., Liu, W., Evans, D. B., Wu, Y., Hicklin, D. J., and Ellis, L. M. (2005). Vascular endothelial growth factor receptor-1 promotes migration and invasion in pancreatic carcinoma cell lines. Cancer *104*, 427-438.

51.   Lichtenberger, B. M., Tan, P. K., Niederleithner, H., Ferrara, N., Petzelbauer, P., and Sibilia, M. (2010). Autocrine VEGF signaling synergizes with EGFR in tumor cells to promote epithelial cancer development. Cell *140*, 268-279.

52.   Naik, S., Dothager, R. S., Marasa, J., Lewis, C. L., and Piwnica-Worms, D. (2009). Vascular Endothelial Growth Factor Receptor-1 Is Synthetic Lethal to Aberrant {beta}-Catenin Activation in Colon Cancer. Clin Cancer Res *15*, 7529-7537.

53.   Hinz, B. (2007). Formation and function of the myofibroblast during tissue repair. J Invest Dermatol *127*, 526-537.

54.   Hinz, B., Phan, S. H., Thannickal, V. J., Galli, A., Bochaton-Piallat, M. L., and Gabbiani, G. (2007). The myofibroblast: one function, multiple origins. Am J Pathol *170*, 1807-1816.

55.   Grivennikov, S. I., Greten, F. R., and Karin, M. (2010). Immunity, inflammation, and cancer. Cell *140*, 883-899.

56.   Grimshaw, M. J., Cooper, L., Papazisis, K., Coleman, J. A., Bohnenkamp, H. R., Chiapero-Stanke, L., Taylor-Papadimitriou, J., and Burchell, J. M. (2008). Mammosphere culture of metastatic breast cancer cells enriches for tumorigenic breast cancer cells. Breast Cancer Res *10*, R52.

57.   Castello-Cros, R., Khan, D. R., Simons, J., Valianou, M., and Cukierman, E. (2009). Staged stromal extracellular 3D matrices differentially regulate breast cancer cell responses through PI3K and beta1-integrins. BMC Cancer *9*, 94.

VITA

High School and Undergraduate Degree Education.

In May of 2000, Jonathon D. Roybal graduated from Franklin High School in El Paso, Texas and attended New Mexico State University as an undergraduate student. He immediately became fascinated by the world of Biology after taking his first introductory courses in science, and he decided to further advance his knowledge of scientific discovery by joining a plant microbiology research lab. He focused on understanding the role of BiP chaperone proteins as a genetic tool to stabilize an essential amino acid, Methionine, in alfalfa. Alfalfa is given to livestock as a source of food and fuel; however, this plant is low in this particular amino acid. Stabilizing the protein would create a genetically modified and enhanced source of food and nutrients for the plant and livestock. The intake of a better food source would increase the health of the livestock and would provide a better source of meat products for people. By performing research, Jonathon gained all the tools and resources he needed to become a better researcher that would be beneficial in years to come. In May of 2005, Jonathon received his Bachelors of Science in Biology with minors in Chemistry and Biochemistry from NMSU. He was accepted into the master's program at the University of Texas Health Science Center at Houston Graduate School of Biomedical Sciences.

Master's Degree Education.

In August of 2005, Jonathon began his classes and research work at University of Texas Health Science Center at Houston Graduate School of Biomedical Sciences. There he joined the lab of Dr. Jonathan M. Kurie, M.D., and began research focused on human lung cancer at U.T. M.D. Anderson Cancer Center. His work led to a first-author publication of a peer-reviewed article in the journal of *Cancer Research* that identified the roles and contributions of stromal cells to lung cancer disease in a mouse tumor model. Jonathon graduated in May of 2008 and decided to work for a year prior to applying for the Ph.D. program at the same school.

Doctoral Degree Education.

In August of 2009, Jonathon began his doctoral thesis laboratory work with Dr. Jonathan M. Kurie, M.D. His doctoral thesis work has led to a first-author publication of a peer-reviewed article in the journal of *Molecular Cancer Research* that identified VEGR1 as a direct target of miR-200 in a murine metastatic lung cancer model. He also demonstrated that carcinoma-associated fibroblasts contribute to the advancement of the disease. Jonathon's work has opened a whole new avenue of research in the field of lung cancer metastasis. Jonathon is eager to use his knowledge and skills to make cancer history, which is the slogan of U.T. M.D. Anderson Cancer Center.

Future Endeavors.

Jonathon is interested in performing a short-term (two year) post-doctoral fellowship program in the field of oral cancer. Jonathon has always been interested in going to dental school and conducting oral cancer research. He hopes to apply his skills and knowledge to making discoveries in the oral cancer field. Jonathon is currently seeking positions throughout the country and is considering applying to multiple dental schools across the country.

Permanent Address:

7417 Le Conte

El Paso, Texas 79912